

# Protein Folding Kinetics: Time Scales, Pathways, and Energy Landscapes in Terms of Sequence Dependent Properties

T. Veitshans<sup>1</sup>, D. K. Klimov<sup>2</sup>, D. Thirumalai<sup>2</sup>

<sup>1</sup> *Laboratoire de Spectrométrie Physique, associé au CNRS*

*Université J. Fourier, Grenoble I; B.P. 87; 38402 Saint-Martin d'Hères Cedex, France*

*and*

<sup>2</sup> *Institute for Physical Science and Technology and Department of Chemistry and Biochemistry*

*University of Maryland, College Park, Maryland 20742, USA*

**Background:** Recent experimental and theoretical studies have revealed that protein folding kinetics can be quite complex and diverse depending on various factors such as size of the protein sequence and external conditions. For example, some proteins fold apparently in a kinetically two state manner whereas others follow complex routes to the native state. We have set out to provide the theoretical basis for understanding the diverse behavior seen in the refolding kinetics of proteins in terms of properties that are intrinsic to the sequence.

**Results:** The folding kinetics of a number of sequences for off-lattice continuum models of proteins is studied using Langevin simulations at two different values of the friction coefficient. We show for these models that there is a remarkable correlation between folding times,  $\tau_F$ , and  $\sigma = (T_\theta - T_F)/T_\theta$ , where  $T_\theta$  and  $T_F$  are the equilibrium collapse and folding transition temperatures, respectively. The microscopic dynamics reveals that several scenarios for the kinetics of refolding arise depending on the range of values of  $\sigma$ . For relatively small  $\sigma$  the chain reaches the native conformation by a direct native conformation nucleation collapse (NCNC) mechanism without being trapped in any detectable intermediates. For moderate and large values of  $\sigma$  the kinetics is described by the kinetic partitioning mechanism (KPM) according to which a fraction of molecules  $\Phi$  (kinetic partition factor) reaches the native conformation via the NCNC mechanism. The remaining fraction attains the native state by off-pathway processes that involve trapping in several misfolded structures. The rate determining step in the off-pathway

processes is the transition from the misfolded structures to the native state. The partition factor  $\Phi$  is also determined by  $\sigma$ : smaller the value of  $\sigma$  larger is  $\Phi$ . The qualitative aspects of our results are found to be independent of the friction coefficient. The simulation results and theoretical arguments are used to obtain estimates for time scales for folding via the NCNC mechanism in small proteins, those with less than about 70 amino acid residues.

**Conclusions:** We have shown that the various scenarios for folding of proteins, and possibly other biomolecules, can be classified solely in terms of  $\sigma$ . Proteins with small values of  $\sigma$  reach the native conformation via a nucleation collapse mechanism and their energy landscape is characterized by having one dominant native basin of attraction (NBA). On the other hand proteins with large  $\sigma$  get trapped in competing basins of attraction (CBA) in which they adopt misfolded structures. Only a small fraction of molecules access the native state rapidly, when  $\sigma$  is large. For these sequences the majority of the molecules approach the native state by a three stage multipathway mechanism, in which the rate determining step involves a transition from one of the CBA's to the NBA.

**Key words:** collapse and folding transition temperature, kinetic partitioning mechanism, native conformation nucleation collapse, protein folding, three-stage multipathway mechanism.

## I. INTRODUCTION

It has become clear over the last few years that the study of minimal models has given rise to a novel theoretical understanding of the kinetics of protein folding [1–8]. The general scenarios that have emerged from these studies are starting to be confirmed experimentally [9–14,33]. In particular, there is now some experimental support [11,14] for the kinetic partitioning mechanism (KPM) first described using minimal off-lattice models [5,15,16]. The principles emerging from these studies have also been used to predict the folding pathways and the nature of kinetic intermediates in specific proteins. For example, it was shown that the single disulfide intermediate 14-38 in bovine pancreatic trypsin inhibitor, which denotes

that the structure of this intermediate contains a covalent disulfide bond between cysteines at location 14 and 38, forms early and decays before other more stable single intermediates start to form [17]. This theoretical prediction has been subsequently verified experimentally [18]. The theoretical studies [1–8,19] have in fact provided, perhaps for the first time, a firm basis for understanding and predicting the overall scenarios that can arise in *in vitro* refolding kinetics of proteins. Since the general scenarios for refolding kinetics have been understood from a qualitative viewpoint it is of interest to correlate in a quantitative manner the dependence of folding times for a number of sequences in terms of parameters that can be *experimentally measured*. In a recent paper theoretical arguments were used to provide quantitative estimate of some of the important time scales that arise naturally according to the KPM [22]. In this paper computational studies are used to complement the previous work. We should note that Onuchic *et al.* have also initiated complementary approaches to understand in a quantitative manner the folding kinetics of small  $\alpha$ -helical proteins [23].

In our earlier work we showed using lattice models that the foldability of proteins (namely, the ability of a sequence with a unique native state to access it in finite time scales under folding conditions) can be understood in terms of two characteristic thermodynamic temperatures which are intrinsic to the sequence [24,25]. One of them is  $T_\theta$ , the collapse transition temperature, at which there is a transition from a random coil to an almost compact state. The other is the folding transition temperature,  $T_F$ , below which the polypeptide chain is predominantly in the native conformation. In the biochemical literature  $T_F$  is roughly the melting temperature,  $T_m$ . It was established for a variety of sequences (in both two and three dimensions) that the folding time correlates extremely well with  $\sigma$  [24,25], where

$$\sigma = \frac{T_\theta - T_F}{T_\theta}. \quad (1)$$

Based on very general arguments [22] it can be shown that  $T_F \leq T_\theta$ , hence  $0 \leq \sigma \leq 1$ . Both  $T_F$  and  $T_\theta$  are sensitive functions of not only the sequence but also the external conditions. This can be verified experimentally and data in the literature in fact support this obvious result. For example, Alexander *et al.* have shown for the IgG binding protein that  $T_F$  (in

their notation  $T_m$ ) varies linearly with pH [26]. These authors have also determined  $T_\theta$  for two forms of IgG binding protein. Thus, foldability of sequences and the associated kinetics for a given sequence can be altered by changing the external conditions. The major purpose of this article is to explore the folding kinetics as a function of  $\sigma$  using off-lattice simplified models of polypeptide chains. In addition, we provide detailed analysis of folding kinetics for a number of sequences at two values of the friction coefficient to assess the role of viscosity on the qualitative aspects of the folding scenarios.

The physical reason for expecting that  $\sigma$  would control the folding rates in proteins is the following. If  $\sigma$  is small, then  $T_\theta \approx T_F$  and hence all the conformations that are sampled at  $T \lesssim T_F$  have relatively high free energy. Any barrier that may exist between these high free energy mobile conformations can be overcome easily provided the temperature at which folding occurs is not too low. Thus, for small  $\sigma$  one can in principle fold a polypeptide chain at a relatively high temperature (in the range where collapse and the acquisition of the native conformation are almost synchronous) and access the native conformation rapidly. For these cases the folding process would appear to be kinetically two state like [20]. Furthermore, studies based on lattice models suggest that for sequences with small and moderate values of  $\sigma$  the kinetic accessibility of the native conformation together with its thermodynamic stability can be achieved over a relatively broad temperature range [24]. On the other hand when  $\sigma \approx 1$ , then  $T_F \ll T_\theta$  and in this case the folding process would inevitably be affected by kinetic traps and misfolded structures. Since some of these misfolded structures can have many elements in common with the native structure they can be fairly stable [15,16]. Since  $T_F$  is low for sequences with large  $\sigma$  these stable structures could have long lifetimes even if the free energy barriers separating them and the native state are only moderate. Thus, it is likely that sequences with  $\sigma \approx 1$  are in general not foldable on biologically relevant time scales. These expectations are borne out in this study and a quantitative relationship between folding rates and  $\sigma$  is given. The energy landscape perspective can be used to argue that small values of  $\sigma$  correspond to the native state having a large native basin of attraction (NBA) [59] or funnel [2,3,27].

Before we close this introduction a brief comment on the use of minimal models to understand folding kinetics is pertinent. This is especially important because their utility in getting insights into protein folding kinetics has been questioned [28]. The minimal models do not explicitly contain all the features that are known to be important in imparting stability to proteins. However, there are many aspects of the minimal models that mimic the dominant interactions in proteins [1]. These involve chain connectivity, hydrophobicity as the driving force, and sequence heterogeneity. In addition, off-lattice models studied in this paper and elsewhere [29,30] which use a realistic representation of the potentials for  $\alpha$ -carbons of a polypeptide chain yield  $(\phi, \psi)$  values consistent with the Ramachandran plot [31]. The aspects of real proteins that are not faithfully represented here are side chains and hydrogen bonds. Straub and Thirumalai have argued that lower order effects like stability arising from hydrogen bonds are included in the simplified off-lattice models of the sort considered here in a coarse grained manner [32]. This is achieved by suitably renormalizing the dihedral angle potentials. Despite these important limitations the studies based on minimal models of proteins have been the only source of concrete testable theoretical predictions in the field of protein folding kinetics [1–8]. Insights based on the energy landscape picture of folding have lead, for example, to the microscopic picture of native conformation nucleation collapse (NCNC) mechanism in refolding of proteins [15,16,19]. Recently, experimentalists have begun interpreting their data on certain proteins [33,34] using the concept of NCNC mechanism. Thus, despite certain limitations these studies have already offered considerable insights into the folding kinetics of biomolecules [1–3,8] in both *in vitro* and *in vivo*.

Since this article is rather lengthy we provide a brief roadmap to the rest of the article. The details of the model and simulation methods are given in Sec. (II) and (III), respectively. The main results are presented in Sec. (IV) and (V). The paper is concluded in Sec. (VI). The appendix contains useful formulae for obtaining time scales for the dominant nucleation collapse process for small proteins. Readers not interested in technical details can skip Sec. (II) and (III) entirely.

## II. DESCRIPTION OF THE MODEL

The model used in our simulations is a variant of the one introduced in our previous studies [15,16]. We use continuum minimal model representation of a polypeptide chain. In these classes of models only the principle features of proteins responsible for imparting stability are retained. These include hydrophobic forces, excluded volume interactions, bond angle and dihedral angle degrees of freedom. The simplified model can be thought of as a coarse grained representation containing only the  $\alpha$ -carbons of the protein molecule. The polypeptide is modeled as a chain consisting of  $N$  connected beads with each corresponding to a set of particular  $\alpha$ -carbons in a real protein. In order to simplify the force field we assume that sequence is essentially built from residues of three types, hydrophobic ( $B$ ), hydrophilic ( $L$ ), and neutral ( $N$ ). Our previous studies have established that the three letter code can be used to construct the basic structural motifs in proteins, namely,  $\alpha$ -helix and  $\beta$ -turns [15,31,35]. In this study we mimic the diversity in the hydrophobic residues in proteins using a dispersion in the interactions between  $B$  residues (see below).

The potential energy of a conformation, which is specified by the set of vectors  $\{\vec{r}_i\}$ ,  $i = 1, 2 \dots N$ , is taken to be of the following form

$$E_p(\{\vec{r}_i\}) = V_{BL} + V_{BA} + V_{DIH} + V_{NON} \quad (2)$$

where  $V_{BL}$ ,  $V_{BA}$ ,  $V_{DIH}$ , and  $V_{NON}$  correspond to bond-length potential, bond-angle potential, dihedral angle potential, and non-bonded potential, respectively. A brief summary of these interactions is given below.

**(a) Bond-length potential.** In our previous studies we assumed that the length of the covalent bond connecting the successive beads to be fixed. The constraint of fixed bond length, which was enforced using the RATTLE algorithm [37], proves to be computationally demanding. In the present study we use a stiff harmonic potential between successive residues, which keeps the bond length approximately fixed, i.e.,

$$V_{BL} = \sum_{i=1}^{N-1} \frac{k_r}{2} (|\vec{r}_{i+1} - \vec{r}_i| - a)^2, \quad (3)$$

where  $k_r = 100\epsilon_h/a^2$ ,  $a$  is the average bond length between two beads, and  $\epsilon_h$ , the average strength of the hydrophobic interaction, is the unit of energy in our model. We have verified that using the potential in Eq. (3) gives the same results for the sequence that has been previously studied [15].

**(b) Bond-angle potential.** The potential for the bending degrees of freedom, describing the angle between three successive beads  $i, i + 1, i + 2$  is taken to be

$$V_{BA} = \sum_{i=1}^{N-2} \frac{k_\theta}{2} (\theta_i - \theta_0)^2, \quad (4)$$

where  $k_\theta = 20\epsilon_h/(rad)^2$  and  $\theta_0 = 1.8326 \text{ rad}$  or  $105^\circ$ .

**(c) Dihedral angle potential.** This potential describes the ease of rotation around the angle formed between four consequent beads. This degree of freedom is largely responsible in determining secondary structures in a polypeptide chain [38]. The  $i^{\text{th}}$  dihedral angle  $\phi_i$  is formed between vectors  $\vec{n}_i = (\vec{r}_{i+1,i} \times \vec{r}_{i+1,i+2})$  and  $\vec{n}_{i+1} = (\vec{r}_{i+2,i+1} \times \vec{r}_{i+2,i+3})$ , i.e., it is the angle between the plane defined by beads  $i, i + 1, i + 2$  and the one spanned by beads  $i + 1, i + 2, i + 3$ . The vector  $\vec{r}_{i,i+1} = \vec{r}_{i+1} - \vec{r}_i$ . The general form of the potential describing the dihedral angle degrees of freedom is well known [39] and can be represented as

$$V_{DIH} = \sum_{i=1}^{N-3} [A_i(1 + \cos \phi_i) + B_i(1 + \cos 3\phi_i)] \quad (5)$$

If two or more of the four beads in defining  $\phi_i$  are neutral ( $N$ ) the  $A_i$  and  $B_i$  are taken to be  $0\epsilon_h$  and  $0.2\epsilon_h$ , respectively. For all other cases  $A_i = B_i = 1.2\epsilon_h$ . For the larger values of  $A_i$  and  $B_i$  the trans state is preferred and this leads to the formation of extended conformation. The presence of neutral residues, which are introduced so that loop formation is facilitated, has the effect of decreasing the barrier and energetic differences between the trans and gauche states [35].

**(d) Non-Bonded potential.** The non-bonded potentials arise between pairs of residues that are not covalently bonded. These forces together with those arising from the dihedral angle degrees of freedom (which provide favorable local interactions for the formation of secondary structures) are responsible for the overall formation of the three dimensional topology of the polypeptide chain.

We take simple forms to represent the non-bonded interaction terms. We assume that the effective potential describing the interaction between the residues  $i$  and  $j$  ( $|i - j| \geq 3$ ) depends on the type of residues involved. The total non-bonded potential is written as

$$V_{NON} = \sum_{i=1}^{N-3} \sum_{j=i+3}^N V_{ij}(r), \quad (6)$$

where  $r = |\vec{r}_i - \vec{r}_j|$ . The potential between two  $L$ -beads or between a  $(L, B)$  pair is taken to be

$$V_{L\alpha}(r) = 4\epsilon_L \left[ \left(\frac{a}{r}\right)^{12} + \left(\frac{a}{r}\right)^6 \right] \quad (\alpha = L \text{ or } B), \quad (7)$$

where  $\epsilon_L = \frac{2}{3}\epsilon_h$ . This potential is purely repulsive with a value of  $2\epsilon_h$  at  $r = 2^{1/6}a$ , which is the location of the minimum in the hydrophobic potential (see Eq. (9)). The presence of  $r^{-6}$  term gives rise to a potential that is longer ranged than the usual  $r^{-12}$  term. The additional term may be interpreted to arise from the hydration shells around the hydrophilic residues.

The interaction between the neutral residues and the others is expressed as

$$V_{N\alpha}(r) = 4\epsilon_h \left(\frac{a}{r}\right)^{12} \quad (\alpha = N, L, \text{ or } B). \quad (8)$$

If both the residues are hydrophobic ( $B$ ) the potential of interaction is taken to be

$$V_{BB}(r) = 4\lambda\epsilon_h \left[ \left(\frac{a}{r}\right)^{12} - \left(\frac{a}{r}\right)^6 \right], \quad (9)$$

where  $\epsilon_h$  determines the strength of the hydrophobic interaction. The above form for  $V_{BB}(r)$  can be thought of as approximate representation (capturing the primary minimum) of the potential of mean force between spherical hydrophobic spheres in water [36].

The dimensionless parameter  $\lambda$  is assumed to have a Gaussian distribution

$$P(\lambda) = \frac{1}{(2\pi\Lambda^2)^{1/2}} \exp\left(-\frac{(\lambda - \lambda_0)^2}{2\Lambda^2}\right), \quad (10)$$

The mean value of  $\lambda_0 = 1$ . The introduction of the distribution in the strength of the hydrophobic interaction creates diversity among hydrophobic species, and hence provides a better caricature of proteins. The standard deviation  $\Lambda$  controls the degree of heterogeneity

of the hydrophobic interactions and if its value becomes too large then the unambiguous division of residues into three distinct types becomes difficult. Consequently, we keep the value of  $\Lambda$  small enough so that the prefactor  $4\lambda\epsilon_h$  is in general greater than  $4\epsilon_L$  (see Eqs. (7,9)). This also assumes that the interaction between hydrophobic residues remains attractive at the separation corresponding to Lennard-Jones minimum. For large values of  $\Lambda$  (not used in our present study) the distribution function in Eq. (10) has to be truncated at some positive value of  $\lambda$  so that the  $\lambda\epsilon_h$  does not become negative.

In our earlier studies [15,16,35] we used  $\Lambda = 0$  and hence all  $B$  beads were identical. Thus, our previous studies correspond exactly to a three letter code. The current potential function with random hydrophobic interaction gives more specificity to the interactions, and yet preserves the overall hydrophobic interactions as the driving force for structure formation.

### III. SIMULATION METHODS

#### A. Langevin dynamics

Following our earlier work we have used Langevin dynamics for simulating folding kinetics [15,35]. We include a damping term in the equation of motion with a properly chosen friction coefficient  $\zeta$  and the Gaussian random force to balance the energy dissipation caused by friction. The equation of motion written for the generalized coordinate  $x$  is given by

$$m\ddot{x} = -\zeta\dot{x} + F_c + \Gamma \equiv F \quad (11)$$

where  $F_c = -\frac{\partial E_p}{\partial x}$  is the conformation force, which is a negative gradient of potential energy with respect to the coordinate  $x$ ,  $\Gamma$  is the random force having a white noise spectrum, and  $m$  is the mass of a bead. The equation of motion Eq. (11) is numerically integrated using the velocity form of the Verlet algorithm [40]. If the integration step is  $h$ , the position of a bead at the time  $t + h$  is expressed through the second order in  $h$  as

$$x(t+h) = x(t) + h\dot{x}(t) + \frac{h^2}{2m}F(t). \quad (12)$$

Similarly, the velocity  $\dot{x}(t+h)$  at the time  $t+h$  is given by

$$\begin{aligned} \dot{x}(t+h) &= \left(1 - \frac{h\zeta}{2m}\right) \left(1 - \frac{h\zeta}{2m} + \left(\frac{h\zeta}{2m}\right)^2\right) \dot{x}(t) + \frac{h}{2m} \left(1 - \frac{h\zeta}{2m} + \left(\frac{h\zeta}{2m}\right)^2\right) \\ &\quad \times \left(F_c(t) + \Gamma(t) + F_c(t+h) + \Gamma(t+h)\right) + o(h^2). \end{aligned} \quad (13)$$

Because we assume that the random force  $\Gamma$  has a white noise spectrum, the autocorrelation function  $\langle \Gamma(t)\Gamma(t') \rangle$  is expressed in the form

$$\langle \Gamma(t)\Gamma(t') \rangle = 2\zeta k_B T \delta(t - t'). \quad (14)$$

Since the equation of motion Eq. (11) is discretized and solved numerically, this formula can be rewritten as

$$\langle \Gamma(t)\Gamma(t+nh) \rangle = \frac{2\zeta k_B T}{h} \delta_{0,n}, \quad (15)$$

where  $\delta_{0,n}$  is the Kronecker delta and  $n = 0, 1, 2, \dots$ . Thus, in the context of this model changing the temperature of the system essentially means changing the standard variance in the Gaussian distribution of the random force  $\Gamma$ .

Temperature is measured in the units of  $\epsilon_h/k_B$ . In the underdamped limit, i.e. when  $\zeta\dot{x}$  is negligible compared to the inertial term in the equation of motion (11), a natural choice of the unit of time is  $\tau_L = (ma^2/\epsilon_h)^{1/2}$ . The simulations have been done in low to moderate friction limit which in the rate theory of reactions would correspond to the energy diffusion regime. The integration step used in the equation of motion is taken to be  $h = 0.005\tau_L$ . All the sequences were studied at two values of the friction coefficient  $\zeta_L = 0.05m\tau_L^{-1}$  and  $\zeta_M = 100\zeta_L = 5m\tau_L^{-1}$ . The relation between the time unit  $\tau_L$  and the folding time scales in real proteins as well as the range of  $\zeta$  used in this study are discussed in the Appendix. The Appendix also gives estimates for certain time scales in the folding kinetics of proteins using the simulation results and theoretical arguments. In our simulations the mass of residue  $m$ , the bond length  $a$ , the hydrophobic energy constant  $\epsilon_h$ , and the Boltzmann constant  $k_B$  are set to unity.

## B. Determination of native conformation

For each sequence we determined the native conformation by adapting the procedure similar to that used in our recent work on lattice model of proteins [24]. The database of sequences generated is described in Sec. (III.D). As in our earlier works [15,35] we have used a combination of slow cooling and simulated annealing to determine the native conformation. The chain is initially heated to  $T = 5.0$  and equilibrated at this temperature for  $2000\tau_L$ . The temperature is then quenched to  $T = 1.0$  and the chain is reequilibrated for an additional  $2000\tau_L$ . This process of quenching the chain from  $T = 5.0$  to  $T = 1.0$  was repeated several times so that we generated a set of independent conformations at  $T = 1.0$ . These structures are used as starting conformations for the slow cooling process. In order to ascertain that the starting conformations are independent the overlap between a pair of these conformations (see Eq. (17)) averaged over all distinct pairs denoted by  $\bar{\chi}$  is calculated. This yields  $\bar{\chi} \sim 0.9$  that roughly corresponds to the value of  $\chi$  for a pair of randomly generated conformations. The temperature of the system in the simulations starting from one of the well equilibrated conformations at  $T = 1.0$ , is slowly decreased to  $T = 0.0$  (see Sec. (III.C) for details). In the process of reaching  $T = 0.0$  the energies of the conformations are recorded. This process is repeated for several (typically 10) initial conformations. The conformation with the lowest energy is assumed to be the native state for the sequence. After determining the native conformation by this method we raised the temperature from 0.0 to 0.2 in  $1000\tau_L$  and then lowered it to  $T = 0.0$ , i.e. we performed a simple simulated annealing procedure. In all instances the resulting structure and the energy coincided with those obtained by the slow cooling protocol. It should be emphasized that this method cannot guarantee that the structures are indeed global energy minima. However, the determination of native structures for these sequences by other optimization techniques leads to the same structures [41]. Thus, we are fairly certain that the structures found by this method indeed are the lowest energy structures for our model.

### C. Thermodynamic properties

We and others have shown that each foldable sequence is characterized by two natural temperatures [1,4,7,15,25]. One of them is  $T_\theta$  below which the chain adopts more or less compact conformation. The transition at  $T_\theta$  is (usually) second order in character suitably modified by a finite size effects. Following our earlier studies  $T_\theta$  is located by determining the temperature dependence of the heat capacity [15,24,25]

$$C_v = \frac{\langle E^2 \rangle - \langle E \rangle^2}{T^2}. \quad (16)$$

The location of the peak in  $C_v$  is taken to be  $T_\theta$ . Previous studies have shown that at  $T \approx T_\theta$  the radius of gyration changes dramatically reaching a value roughly coinciding with that for a compact conformation [15,35]. This, of course, is usually taken to be a signature of "collapse" transition in homopolymers [42].

The second crucial temperature is the folding transition temperature  $T_F$ . There are several ways of calculating  $T_F$  all of which seem to give roughly similar estimates [7,25,47]. We use the fluctuations in the structural overlap function to estimate  $T_F$ . The structural overlap function is defined as

$$\chi = 1 - \frac{2}{N^2 - 5N + 6} \sum_{i=1}^{N-3} \sum_{j=i+3}^N \Theta(\varepsilon - |r_{ij} - r_{ij}^N|), \quad (17)$$

where  $r_{ij}$  is the distance between the beads  $i$  and  $j$  for a given conformation,  $r_{ij}^N$  is the corresponding distance in the native conformation, and  $\Theta(x)$  is the Heavyside function. If  $|r_{ij} - r_{ij}^N| \leq \varepsilon$  then the beads  $i$  and  $j$  are assumed to form a native contact. In our simulations we take  $\varepsilon = 0.2a$ .

It follows from the definition of  $\chi$  that at finite temperatures  $\langle \chi(T) \rangle$ , the thermal average, is in general non-zero. The folding transition temperature is obtained from the temperature dependence of the fluctuations in  $\chi$

$$\Delta\chi = \langle \chi^2(T) \rangle - \langle \chi(T) \rangle^2 \quad (18)$$

For sequences with a unique ground state  $\Delta\chi$  exhibits a peak at  $T \simeq T_F$  [25]. It has been shown that for these simple off-lattice models this transition is a finite size first order phase transition [15]. Our previous lattice model studies have shown that  $T_F$  obtained from the temperature dependence of  $\Delta\chi$  is in general slightly smaller than that calculated from the midpoint of  $\langle \chi(T) \rangle$  or other suitable order parameters [43].

The thermodynamic properties like  $\langle \chi(T) \rangle$ , total energy  $\langle E(T) \rangle$  (the sum of kinetic and potential energies) etc. are calculated using time averages over sufficiently long trajectories. The trajectories which are generated in the search for the native structure can be used to get an approximate estimate of the temperature interval  $(T_l, T_h)$ , which includes the temperatures  $T_\theta$  and  $T_F$ . In all cases we set  $T_h = 1.0$ , while  $T_l$  varies from 0.3 to 0.4. Each trajectory starts with the same zigzag initial conformation. The chain is then heated at  $T = 5.0$  and brought to equilibrium at  $T = 1.0$  as described in Sec. (III.B). The method of slow cooling employed for calculating thermodynamic averages is identical to that presented in [43]. The system is periodically cooled (starting at the temperature  $T_h$ ) by an amount  $\Delta T$ . The time  $\tau_{max}$  is the time of running the simulations at the fixed temperature,  $T_i = T_h - i\Delta T$ , where  $i = 0, 1, 2, \dots$ . In this study we have set  $\Delta T = 0.02$ , the time  $\tau_{max} = 2500\tau_L$ , and the equilibration time after the change of the temperature by  $\Delta T$  to be  $\tau_{eq} = 250\tau_L$ . These values are used with most sequences within the entire temperature interval  $(T_l, T_h)$ . The thermodynamic values for one particular initial condition  $i$  is calculated as

$$\overline{f}_i(T) = \frac{1}{\tau_{av}} \int_{\tau_{eq}}^{\tau_{eq} + \tau_{av}} f_i(T, t) dt, \quad (19)$$

where  $\tau_{av} = \tau_{max} - \tau_{eq}$ . The equilibrium thermodynamic value is obtained by averaging over a number of initial conditions

$$\langle f(T) \rangle = \frac{1}{M} \sum_{i=1}^M \overline{f}_i(T). \quad (20)$$

We found that  $M = 50$  was sufficient to obtain accurate results for equilibrium properties. For most sequences the values of parameters (see above) used in the course of equilibration

were large enough to obtain converged results. In some instances the equilibration times had to be increased to obtain converged results. The functions  $\langle E(T) \rangle$ ,  $C_v(T)$ , and  $\Delta\chi(T)$  are obtained by fitting the data by polynomials, and  $\langle \chi(T) \rangle$  was fit with two hyperbolic tangents.

We should note that due to the intrinsic heterogeneity of these systems non-ergodicity effects often manifest themselves [15]. If this is the case, we need to do weighted averaging of thermodynamic quantities, as described elsewhere [15,44], to get converged results. This issue was not encountered for the sequences that were examined in this study.

It is obvious that the thermodynamic quantities are independent of the underlying dynamics provided the dynamics yields the Boltzmann distribution at  $t \rightarrow \infty$ . Since the thermodynamics is only determined by the Boltzmann factor  $\exp(-E_p/k_B T)$  it is convenient to determine them at low friction where the sampling of conformation space appears to be more efficient [15,35].

#### D. Database of sequences

For our model one can, in principle, generate infinite number of sequences because of the continuous distribution of the effective hydrophobic interactions (see Eq. (10)). The vast majority of such sequences would be random, and hence would not fold to a unique native state on finite time scale. Our goal is to obtain a number of these sequences with the characteristic temperatures  $T_\theta$  and  $T_F$  such that they span a reasonable range of  $\sigma$  (see Eq. (1)). It is clear that merely creating random sequences will not achieve this objective. In general, random sequences would take extraordinarily long times to fold. It is known that foldable sequences (those that reach the native state in finite times) are designed to have a relatively smooth energy landscape. Such sequences may, in fact, be minimally frustrated [45] or have compatible long and short-range interactions [57]. Thus, in order to generate sequences that span the range of  $\sigma$  and which are foldable, we used the most primitive design procedure in the inverse protein folding problem [49,50]. Because our objective is

not to provide the most optimal solution to the inverse folding problem the more reliable methods introduced recently were not utilized [51].

In all our studies the number of beads  $N = 22$ . The composition of all sequences is identical, namely, all of them contain 14 hydrophobic beads, 5 hydrophilic beads, and 3 neutral beads. The sequences in this model differ from each other because of the precise way in which these beads are connected. In addition, due to the distribution of hydrophobic interactions not all hydrophobic beads are identical. The latter condition also introduces diversity among sequences.

The method for creating the database of sequences is as follows. The first sequence  $A$ ,  $B_9N_3(LB)_5$ , examined has been already studied in our previous work [15]. This allows us to ascertain that our modified model (incorporating stiff harmonic bond-length potential instead of RATTLE algorithm) yields results consistent with our earlier studies. This sequence has zero  $\Lambda$ , so all hydrophobic residues are identical. All other sequences (to be used as starting conditions for Monte Carlo optimization procedure, see below) were generated at random with different standard deviations  $\Lambda$ , but preserving the same composition, i.e. 14  $B$  beads, 5  $L$  beads, and 3  $N$  beads. By "random generation" of a sequence we mean that a sequence is randomly constructed from the beads of three types and the values of the parameter  $\lambda$  specifying non-bonded interactions between hydrophobic residues in a sequence (Eq. (9)) were obtained using Gaussian distribution Eq. (10). Specifically, we used  $\Lambda = 0$  (one sequence),  $\Lambda = 0.1$  (one sequence),  $\Lambda = 0.17$  (one sequence),  $\Lambda = 0.3$  (five sequences).

The next step in creating the database of sequences is the choice of the target conformation, the precise choice of which is rather arbitrary because the only natural requirement is that it should be compact. However, due to intrinsic propensity toward bend formation near clusters of  $N$  residues, it seems reasonable to restrict the choice of target conformation topology to that with single U-turn. Obviously, the number of residues in a sequence  $N = 22$  allows us to define much more complicated topologies featuring multiple U-turns. In order to avoid the comparison of folding behavior of the sequences with the native conformations of different topologies the only criterion for selecting target conformations is that they must

have a single U-turn and be reasonably compact. The role of the topology of the ground state in determining the folding kinetics will be addressed in a future paper. Thus, using the conditions described above we have selected the target conformations from the database of low energy structures found in the course of slow cooling simulations.

Once a target conformation is chosen Monte Carlo algorithm in sequence space [49,50] is used to obtain an optimal sequence by means of the primitive inverse design procedure, i.e., the sequence that has the lowest energy and is compatible with the target conformation. There is no guarantee that this procedure is by any means the best way of designing optimal sequences as has been pointed out by Deutsch and Kurosky [51]. However, for our purposes this naive procedure suffices. The main idea is to perform small random permutations of a sequence while keeping its composition fixed and accepting (or rejecting) new sequences with respect to the Boltzmann factor  $P = \exp(-\Delta E/k_B T)$ , where  $\Delta E$  is the energy variation due to permutation and  $T$  is the temperature of Monte Carlo optimization scheme [49,50]. Hence, this algorithm is aimed at lowering the energy of the target conformation. The sequence providing the lowest energy at the target conformation is chosen as the desired sequence and used for further analysis. The control parameter which specifies the degree (or "quality") of optimization is the temperature  $T$ . For most sequences we have used low value of  $T = 0.2$ . We have made several attempts to run Monte Carlo algorithm in a sequence space by gradually decreasing the temperature from high values of  $T \gtrsim 1.0$  up to the very low values  $T \lesssim 0.01$ . This method, however, does not often provide lower energies of target conformations than that based on quenching the temperature at a certain value, and this is probably due to moderate ruggedness of the energy landscape in sequence space. It must be emphasized that the optimization scheme does not guarantee that the target conformation is actually the native state of the optimized sequence. This should be checked in the course of molecular dynamics simulations (see below).

The nine sequences obtained using the procedure described above are listed in Table 1 and are labeled A through I. Of the nine sequences eight (B-I) were generated using Monte Carlo method in sequence space. All sequences have different native conformations, except

the pairs of sequences A,D and B,C, which share the same native state. It must also be emphasized that although sequences F-H have identical distribution of beads they differ from each other with respect to the strength of hydrophobic interactions, i.e. they have different sets of prefactors  $\lambda$  (Eq. (10)).

### E. Simulation temperature

In order to compare the rates of folding for different sequences it is desirable to subject them to identical folding conditions. The equilibrium value of  $\langle \chi(T) \rangle$  measures the extent to which the conformation at a given temperature  $T$  is similar to the native state. At sufficiently low temperature  $\langle \chi(T) \rangle$  would approach zero, but the folding time may be far too long. We chose to run our folding simulations at a sequence dependent simulation temperature  $T_s$  which is subject to two conditions: (a)  $T_s$  be less than  $T_F$  for a specified sequence so that the native conformation has the highest occupation probability; (b) the value of  $\langle \chi(T = T_s) \rangle$  be a constant for all sequences, i.e.

$$\langle \chi(T = T_s) \rangle = \alpha. \quad (21)$$

In our simulations we choose  $\alpha = 0.26$  and for all the sequences studied  $T_s/T_F < 1$ . This general procedure for selecting the simulation temperatures has been already used in recent studies of folding kinetics using lattice models [43,46,47].

An alternative way of choosing  $T_s$  is to assume that the probability of occupation of the native state be the same for all sequences. In our previous study [43] on lattice models we have used this method for a small number of sequences. The trends in the folding times at the resulting simulation temperatures (as well as the kinetics) were very similar to those found when Eq. (21) is used to determine  $T_s$ .

It is also possible to keep the simulation temperature constant for all sequences. Because  $T_F$  and  $T_\theta$  vary greatly depending on sequence such a choice would not ensure that the probability of being in the native conformation is roughly the same for all sequences or

that all sequences are qualitatively similar to the same extent. In other words the folding conditions for the sequences would effectively be different if the temperature is held constant. This argument also implies that the statistical trends of folding kinetics with respect to intrinsic sequence dependent properties are expected to hold only over an optimal range of folding conditions which in simulations are entirely determined by temperature.

## F. Monitoring folding kinetics

The simulation procedure for obtaining folding kinetics resembles the slow cooling method apart from the one principal difference that after heating the chain it is quenched to the temperature  $T_s$ , defined from the condition  $\langle \chi(T = T_s) \rangle = 0.26$ . The temperature is held constant after the quench to  $T = T_s$ . The duration of the folding simulations depends on the rate of folding of a particular sequence and is typically on the order of  $10^4 \tau_L$ . For each sequence we generated between 100 – 300 independent trajectories. The folding kinetics is monitored using the fraction of trajectories  $P_u(t)$  which does not reach the native conformation at time  $t$

$$P_u(t) = 1 - \int_0^t P_{fp}(s) ds, \quad (22)$$

where  $P_{fp}(s)$  is the distribution of first passage times,

$$P_{fp}(s) = \frac{1}{M} \sum_{i=1}^M \delta(s - \tau_{1i}). \quad (23)$$

In Eq. (23)  $\tau_{1i}$  denotes the first passage time for the  $i^{\text{th}}$  trajectory, i.e. the time when a sequence adopts native state for the first time. It is easy to show that the mean first passage time  $\tau_{MFPT}$  to the native conformation (which is roughly the folding time,  $\tau_F$ ) can be calculated as

$$\tau_{MFPT} = \int_0^\infty t P_{fp}(t) dt = \int_0^\infty P_u(t) dt. \quad (24)$$

The mean first passage time  $\tau_{MFPT}$  can also be calculated using  $\tau_{1i}$  for the  $M$  trajectories so that

$$\tau_{MFPT} = \frac{1}{M} \sum_{i=1}^M \tau_{1i}. \quad (25)$$

We find that for all the sequences  $P_u(t)$  can be adequately fit with several exponentials of the form

$$P_u(t) = \Phi \exp\left(-\frac{t}{\tau_{FAST}}\right) + \sum_k a_k \exp\left(-\frac{t}{\tau_k}\right), \quad (26)$$

where the sum is over the dominant misfolded structures,  $\tau_k$  are the time scales for activated transition from one of the misfolded structures to the native state, and  $\sum_k a_k = 1 - \Phi$ . In this study we report  $\tau_{MFPT}$  using Eq. (24) by fitting  $P_u(t)$  according to Eq. (26). We have explicitly verified that Eq. (24), with  $P_u(t)$  given by Eq. (26), and Eq. (25) yield practically identical results.

It has been shown in a series of articles that multiexponential fit of the function  $P_u(t)$  can be understood in terms of the kinetic partitioning mechanism [8,15,16,19] and is indicative of the distribution of time scales in the refolding of biomolecules. According to KPM a fraction of molecules  $\Phi$  folds to the native conformation very rapidly, while the remainder  $(1 - \Phi)$  approaches the native state via a complex three stage multipathway mechanism (TSMM). Therefore, the time constants  $\tau_{FAST}$  and  $\tau_k$  can be interpreted as the characteristic folding times of the fast and slow phases, respectively. When appropriate fit of the function  $P_u(t)$  with exponentials is performed, the calculation of the mean first passage time  $\tau_{MFPT}$  becomes straightforward.

An alternative way to calculate folding times is based on the analysis of the time dependence of the overlap function. The overlap function  $\chi$  is constantly calculated during simulations and its average time dependence is obtained as

$$\langle \chi(t) \rangle = \frac{1}{M} \sum_{i=1}^M \chi_i(t), \quad (27)$$

where  $\chi_i(t)$  is the value of  $\chi$  for the  $i^{\text{th}}$  trajectory at time  $t$ . We find that  $\langle \chi(t) \rangle$  can also be fit by a sum of exponentials (usually by one or two, see [24,25])

$$\langle \chi(t) \rangle = a_1 \exp\left(-\frac{t}{\tau_1}\right) + a_2 \exp\left(-\frac{t}{\tau_2}\right) \quad (28)$$

Here  $\tau_1$  gives the estimate for the time scale of native conformation nucleation collapse process [15,16], while the largest time constant in the fit  $\tau_2$  serves as an estimate of the folding time  $\tau_F$ . For most sequences biexponential fit provides the most accurate results. However, several sequences (typically ones with relatively small values of  $\sigma$ ) demonstrate a clear single exponential behavior of  $\langle \chi(t) \rangle$ . In some cases there are additional slow components present on larger time scales as well. It has been shown in our previous papers that defining folding times using the functions  $P_u(t)$  or  $\langle \chi(t) \rangle$  yields qualitatively similar results [15,43]. The same conclusion is valid for this model as well. Thus,  $\tau_{FAST}$  and the largest  $\tau_k$  in Eq. (26) are roughly proportional to  $\tau_1$  and  $\tau_2$ , respectively.

## IV. RESULTS

### A. Thermodynamic properties

In this section we present the results on thermodynamics and kinetics of folding. Using the methodology described above, we studied 9 sequences, 8 of which were generated by performing Monte Carlo simulations in sequence space. The native conformation of each sequence was determined using the procedure described in Sec. (III.B). The example of the native conformation for the sequence G is given in Fig. (1). This picture demonstrates that all three neutral residues shown in grey are concentrated in the turn region. It is also clearly seen that hydrophobic residues shown in blue tend to be in close contact to each other due to their inherent attractive interaction, while hydrophilic residues shown in red point outwards.

For each sequence we calculated the two characteristic equilibrium temperatures, collapse transition temperature  $T_\theta$  and folding transition temperature  $T_F$  from the temperature dependence of  $C_v$  and  $\Delta\chi$ , respectively. The plots of  $\langle \chi \rangle$  and  $\langle E \rangle$  were also obtained. Fig. (2) displays these functions for the sequence G. The plot of  $\langle \chi(T) \rangle$  in Fig. (2a) indicates that at high temperatures  $0.8 \lesssim T \lesssim 1.0$  the value of  $\langle \chi \rangle \approx 0.8$ , so the chain has

negligible amount of the native structure. It was already shown in [35] that under these conditions polypeptide chain is in a random coil conformation. The overlap function gradually decreases with the temperature and at  $T = 0.3$  it reaches the value below 0.2. We do not plot  $\langle \chi \rangle (T)$  for  $T < 0.3$ , because at such low temperatures it is difficult to obtain reliable thermodynamic averages due to non-ergodicity problems. Fortunately, this is not necessary for the aim of our study because all characteristic temperatures  $T_\theta$ ,  $T_F$  and the simulation temperature  $T_s$  are relatively high. The peak of the specific heat  $C_v$  (see Fig. (2d)) which corresponds to the collapse transition temperature  $T_\theta$  is at 0.78. At this temperature protein undergoes a transition from an extended coil state to compact conformation. In fact, we calculated the radius of gyration  $\langle R_g^2 \rangle$  as a function of temperature for few sequences and found that at  $T \approx T_\theta$  it shows a sudden drop in accord with earlier and more recent studies [15,35]. However, at  $T_\theta$  the overlap function is still relatively large ( $\langle \chi \rangle \approx 0.7$ ). The fluctuation of the overlap function  $\Delta\chi$  achieves a maximum at  $T = 0.62$  and this is taken to be the folding temperature  $T_F$ . The value of  $T_F$  calculated from the midpoint of  $\langle \chi \rangle$  (i.e., when  $\langle \chi \rangle$  is about 0.5) is also around 0.62. In general, we have found that  $T_F$  obtained from the peak of  $\Delta\chi$  is slightly lower than that calculated from the temperature dependence of similar measures like  $\langle \chi \rangle$  [43]. It was demonstrated that this temperature corresponds to first order folding transition to the native conformation [15,25]. By monitoring  $\chi(t)$  for several individual trajectories under equilibrium conditions at  $T \approx T_F$  we find that the protein fluctuates between the native and disordered conformations. All the nine sequences show similar behavior from which the various thermodynamic parameters can be easily extracted. The parameter  $\sigma$  (see Eq. (1)) for the nine sequences ranges from 0.14 to 0.65. Thus, a meaningful correlation between the folding time and  $\sigma$ , which is one of the major purposes of this study, can be established.

The simulation temperature  $T_s$  for the sequence G defined by Eq. (21) is found to be 0.41. In Fig. (3) we present the dependence of  $T_s$  on the parameter  $\sigma$ . It is seen that the simulation temperature  $T_s$  is a decreasing function of  $\sigma$ . Thus, high values of  $T_s$  are found for the sequences with small values of  $\sigma$ , and this prompts us to anticipate that such

sequences are fast folders (see below). However, it was argued [43] that this correlation must be viewed as statistical. This implies that if two sequences have close values of  $\sigma$ , then a precise correlation with  $T_s$  is not always expected. On the other hand, if a large number of sequences spanning a range of  $\sigma$  is generated, then we expect a statistical correlation to hold. We also expect these conclusions to hold over a range of temperatures which is favorable for folding. The present off-lattice studies and those based on lattice models [24,43] confirm this expectation.

### B. Dependence of $T_\theta$ and $T_F$ on sequence

One of the major results in this study (see Sec. (IV.D)) is that the folding times for all sequences correlate extremely well with  $\sigma$  (cf. Eq. (1)). Therefore, it is of interest to investigate how  $T_\theta$  and  $T_F$  vary with the sequence. It seems reasonable to assert that the folding temperature  $T_F$  depends rather sensitively on the precise sequence. In fact, it has been argued that to a reasonable approximation  $T_F$  is determined by the nature of the low energy spectrum (a sequence dependent property), at least in lattice models [48]. The sensitive dependence of  $T_F$  on the sequence is explicitly confirmed in the present paper and in the previous lattice models as well [43,48]. In Table 1 we display  $T_F$  for the nine sequences. The values of  $T_F$  range from 0.20 to 0.62. Thus, the largest  $T_F$  is about three times larger than that of the smallest value.

It might be tempting to think that  $T_\theta$  should be insensitive to the sequence and should essentially be determined by the composition of the sequence. This expectation arises especially from heteropolymer theory [52]. According to the heteropolymer model, which essentially ignores short length scale details,  $T_\theta$  is determined by the average excluded volume interactions,  $v_0$ , and the average strength of hydrophobic interactions,  $\lambda_0\epsilon_h$ . Both these values are expected to be roughly constant, especially if the sequence composition is fixed. The determination of  $T_\theta$  for a polypeptide chain based on these arguments ignores surface terms and may, in fact, be valid in the thermodynamic limit, i.e. when the number of

beads tends to infinity. However, polypeptide chains are finite sized and hence the nature of surface residues which depends on the precise sequence are critical in the determination of  $T_\theta$ . This, in fact, is borne out in our simulations. In Table 1 we also display  $T_\theta$  for the nine sequences. Although the largest  $T_\theta$  is only approximately 1.5 times (as oppose to a factor of three for  $T_F$ ) larger than that of the lowest it is clear that  $T_\theta$  is very sequence dependent even though the composition for all sequence is identical. All the sequences have 14 hydrophobic residues. Thus, both  $T_\theta$  and  $T_F$  are determined not only by the intrinsic sequence but also by external conditions. In fact,  $T_\theta$  and  $T_F$ , and, consequently,  $\sigma$  can be manipulated by altering the external solvent conditions (pH, salt, etc.). It therefore follows that a single foldable sequence can have very different values of  $\sigma$  depending on the solvent conditions and hence can exhibit very different kinetics.

It is interesting to obtain estimates for  $T_\theta$  and  $T_F$  using realistic values of  $\epsilon_h$ , the average strength of hydrophobic interaction. From Table 1 we note that the range of  $T_\theta$  is  $(0.58 - 0.80)\epsilon_h/k_B$  with the lower values corresponding to sequences with larger  $\sigma$ . The value of  $\epsilon_h$  ranges from  $(1 - 2)kcal/mol$ . Assuming that  $\epsilon_h \approx 2kcal/mol$  the range of  $T_\theta$  is  $(48 - 67)^\circ C$ . It appears that the better designed sequences (ones with smaller  $\sigma$  values) have more realistic values of  $T_\theta$ . Similarly the range of  $T_F$  for better designed sequences is  $(33 - 50)^\circ C$ . These estimates suggest that optimized sequences can fold over a moderate range of temperatures rapidly and with relatively large yield. These expectations are explicitly demonstrated here.

### C. Kinetics of folding: The Kinetic Partitioning Mechanism (KPM)

We studied the folding kinetics using the function  $P_u(t)$ , which gives the fraction of unfolded molecules (trajectories) at time  $t$ . We also computed the time dependence of  $\langle \chi(t) \rangle$  to gain additional kinetic information concerning the approach to the native conformation. The function  $P_u(t)$  has been obtained for each sequence at the simulation temperature  $T_s$  from the analysis of large number of individual trajectories ( $M = 100 - 300$ ) starting with different initial conditions. The resulting plots of  $P_u(t)$  were fitted with a sum

of exponentials (one, two, or three) and the mean first passage time  $\tau_{MFPT}$  (taken to be equal to  $\tau_F$ ) for each sequence was calculated as described in Sec. (III.F). In general, it is found that after a short transient time  $P_u(t)$  is extremely well fit by a sum of exponentials (cf. Eq. (26)). The partition factor,  $\Phi$ , gives the fraction of molecules that reaches the native conformation on the time scale  $\tau_{FAST}$  by a NCNC mechanism and  $\tau_k$  ( $\gg \tau_{FAST}$ ) being the time scales over which the remaining fraction  $1 - \Phi$  reaches the native state [15,16,43].

Based on fairly general theoretical considerations it has been shown that  $\sigma$  ( $= (T_\theta - T_F)/T_\theta$ ) can be used to discriminate between fast and slow folding sequences [25,22]. This has been confirmed numerically for lattice models [24,43,48]. We classify fast folding sequences as those with relatively large values of  $\Phi$  ( $\gtrsim 0.9$ ). These sequences reach the native conformation without forming any discernible intermediates and essentially display a two state kinetic behavior. The plot of  $P_u(t)$  for one of these sequence (sequence G) which can be fit with only one exponential in Eq. (26) is presented in Fig. (4a). It is obvious that  $\Phi$  depends on the sequence (via  $\sigma$ ), the temperature, and other external conditions. Four sequences out of nine appear to be fast folders displaying a two state kinetic approach to the native conformation with  $\Phi \gtrsim 0.9$ . These sequences have  $\sigma$  values less than about 0.4.

The other five sequences have  $\Phi$  values less than 0.9 and hence can be classified as moderate or slow folders. The values of  $\sigma$  for these sequences exceed 0.4. The discrimination of sequences into slow and fast based on  $\Phi$  is arbitrary. An example of the kinetic behavior of a slow folder (sequence A) probed using  $P_u(t)$  is shown in Fig. (4b). The generic behavior of  $P_u(t)$  as a sum of several exponentials has been argued to be a consequence of the kinetic partitioning mechanism [15,22]. Typically for slow folding sequences  $\tau_{FAST}$  varies from  $200\tau_L$  to  $600\tau_L$ , whereas the largest value of  $\tau_k$  (as defined by Eq. (26)) lies in the interval from  $2500\tau_L$  to  $2.7 \times 10^6\tau_L$ . Slow folding trajectories reach the native state via three stage multipathway mechanism [15,22,25], according to which random collapse of a protein (first stage) is followed by a slow search of the native state among compact conformations (second stage) that eventually leads the polypeptide chain to one of several misfolded structures. These misfolded structures have many characteristics of the native state. Generically the

rate determining step in the TSMM involves the transition (crossing a free energy barrier) from the misfolded structure to the native state (third stage) [25].

In order to obtain insights into the microscopic origins of the slow and fast phases we have analyzed the dynamic behavior of various trajectories. We have found that for sequences that find the native conformation essentially in a kinetically two state manner all the trajectories reach the native conformation without forming any discernible intermediates. Furthermore, for these cases once a certain number of contacts is established the native state is reached very rapidly, which is reminiscent of a nucleation process [6,15,16]. The time scale for such nucleation dominated processes is relatively short and it has been suggested that in these cases the collapse process and the acquisition of the native conformation occur almost simultaneously [22]. It is for this reason we refer to this process as native conformation nucleation collapse (NCNC). This process has been referred to as nucleation condensation mechanism by Fersht [10]. These points are illustrated by examining the dynamics of the structural overlap function  $\chi(t)$  for fast folders. A typical plot for  $\chi(t)$  for a fast folder (sequence G) is shown in Fig. (5). In Fig. (5) (as well as in Figs. (6-8,15,16)) we plot  $\chi(t)$  for a trajectory labeled  $k$  averaged over a few integration steps  $h$ , i.e.,

$$\overline{\chi}_k(t) = \frac{1}{\overline{\tau}} \int_{t-\overline{\tau}/2}^{t+\overline{\tau}/2} \chi_k(s) ds. \quad (29)$$

The value of  $\overline{\tau} = 5\tau_L$  which is much less than any relevant folding time scales. This figure (Fig. (5a)) shows that within  $380\tau_L$  (the first passage time) the chain reaches the native conformation. After the chain reaches the native state there are fluctuations around the equilibrium value of  $\langle \chi \rangle (= 0.26)$ . Another example of folding trajectory for this sequence is presented in lower panel, which is further analyzed in Sec. (IV.D).

The dynamical behavior shown in Fig. (5) for fast trajectories should be contrasted with the trajectories for other sequences that reach the native state by indirect off-pathway processes. An example of such a behavior for the moderate folder (sequence E,  $\Phi = 0.72$ ) is shown in Fig. (6). The behavior presented in Fig. (6a) shows that after an initial rapid collapse (on the time scale of about  $100-200\tau_L$ ) the chain explores intermediate state (where

$\chi(t)$  is roughly constant for a large fraction  $\tau_I/\tau_{1i}$  of time, where  $\tau_I$  is the life-time of the intermediate state) before reaching the native conformation at  $\tau_{1i} = 3026\tau_L$ . Fig. (6b) shows another off-pathway trajectory for this sequence, in which native conformation is reached at  $1970\tau_L$ . Although these slow trajectories are qualitatively similar, they clearly demonstrate that the chain samples different misfolded conformations depending on the initial conditions before it finally finds the native state. This fact further supports the multipathway character of the indirect folding process. After the native conformation is reached the overlap function fluctuates around the equilibrium value  $\langle \chi \rangle = 0.26$  or makes sudden jumps to the higher values of  $\chi \approx 0.4$  and fluctuates around these values for a finite time. Such dynamics clearly reflects frequent visits to low lying structures (see Sec. (IV.D)). The behavior shown in Fig. (6) is very typical of the trajectories that reach the native conformation via indirect mechanisms which are conveniently quantified in terms of TSMM. Fig. (7) presents a typical indirect trajectory for fast sequence I, which has the partition factor  $\Phi$  slightly less than unity. This trajectory reaches the native conformation at  $2384\tau_L$ .

It is also instructive to compare the dynamical behavior of the nucleation trajectories of fast and slow folding sequences. An example of a trajectory that reaches the native conformation via nucleation collapse mechanism for sequence E is shown in Fig. (8). It is important to note that the qualitative behavior of  $\chi(t)$  presented in Fig. (8) is very similar to that shown in Fig. (5). This further confirms that the underlying mechanism that leads the chain directly to the native conformation for sequences with large  $\sigma$  is similar to the nucleation process. The only difference is that the partition factor  $\Phi$  is less for sequences with large  $\sigma$  than for ones with small  $\sigma$ . Fig. (8) also indicates that after reaching native state the chain makes frequent visits to neighboring misfolded conformations and, in some instances, gets trapped in these for relatively long times.

The kinetic behavior described above suggests that the value of  $\sigma$  can be used to classify sequences according to their ability to access the native state. It appears that not only does  $\sigma$  correlate well with the intrinsic kinetic accessibility of the native conformation it also statistically determines the kinetic partition factor  $\Phi$ . In Fig. (9a) we show the dependence

of  $\Phi$  on  $\sigma$  for the nine sequences. The trend which emerges from this plot is that the sequences with larger values of  $\sigma$  (and consequently with larger  $\tau_{MFPT}$ ) have smaller values of  $\Phi$ . For example, for the slow folding sequence labeled A with the largest value of  $\sigma = 0.65$  the fraction of fast trajectories is  $\Phi = 0.43$ . In contrast, the fastest folding sequence labeled I ( $\sigma = 0.14$ ) for which biexponential fit of  $P_u(t)$  is needed, has the value of  $\Phi \gtrsim 0.9$ .

#### **D. Probes of kinetic and equilibrium intermediates using inherent structures: Roles of NBA and CBA**

The question of the nature and relevance of intermediates in protein folding is of abiding interest. Our studies here and elsewhere [22,43] have demonstrated that the scenarios for folding can be conveniently classified in terms of  $\sigma$  provided the foldable sequences are compared in a similar manner. In order to probe the role of intermediates in the approach to native state we have analyzed three sequences (E, G, and I) using the kinetic order parameter profiles. Sequences G and I are classified as fast folders (the partition factor  $\Phi$  exceeds 0.9) while sequence E is a moderate folder with the associated  $\sigma$  ( $\Phi = 0.72$ ) lying in the boundary between fast and slow folding sequences.

We analyze the role of kinetic and equilibrium intermediates (defined below) using the following methodology. Each trajectory is divided into a kinetic part and an equilibrium part. The kinetic part of a trajectory labeled  $i$  includes the portion from the beginning till the native state is reached for the first time, namely, the first passage time,  $\tau_{1i}$ . The equilibrium part is taken to be the remaining portion of the trajectory from  $\tau_{1i}$  till  $\tau_{max}$ . For convenience we take  $\tau_{max}$  to be the same for all trajectories. In order to characterize the nature of intermediates we use the overlap function,  $\chi$ , which, as described earlier, gives the degree of similarity to the native conformation. It is possible that the same value of  $\chi$  may correspond to different conformations and in some instances to conformations that are even structurally unrelated to each other. However, by studying the distribution of overlap function over a range of  $\chi$  for several independent initial conditions and by directly comparing the resulting

conformations and calculating  $\chi$  between them we can ascertain the states that are visited with overwhelming probability before and after reaching the native conformation. In order to probe the nature of kinetic and equilibrium intermediates that the chain samples en route to the native conformation we have determined the "inherent" structures [58] (see below). The inherent structures are obtained from the time course of  $\chi(t)$  examples of which are shown in Figs. (5-8). The basins of attractions are obtained before the chain reaches the native conformation for the first time (i.e., the "kinetic" basins) and are determined as follows. As the polypeptide chain approaches the native conformation (but has not yet reached it, i.e.,  $t < \tau_{1i}$ ), we record several (usually about 10) instantaneous conformations which serve as initial conditions for steepest descent simulations. In this method the temperature is set to zero and the velocities of all residues are rescaled to zero after each integration step. This results in a "downhill" motion of a sequence on the energy surface. The final conformations of the steepest descent quench simulations (provided they are sufficiently long) are the conformations of local energy minima (inherent structures) which the sequence explores in the folding process. These conformations obtained at different times and with distinct initial conditions allow us to map the distribution of folding pathways. The same technique for getting inherent structures was used after the first passage time  $\tau_{1i} < t < \tau_{max}$  as well. These would give us the "equilibrium" intermediates. This analysis allows to compare the nature of intermediates in the kinetic pathways.

For sequence G we determined the inherent structures using the instantaneous conformations labeled (1-6) (all of which occur at  $t < \tau_{1i}$ ) shown in Fig. (5b). The inherent structures for this particular trajectory (and for others as well) almost always coincide with the native state. This clearly shows that for sequence G, for which the native state is reached by the nucleation collapse mechanism, the various inherent structures directly map into the native basin of attraction (NBA). The rapid approach to the NBA is the reason for the two state kinetics displayed. It also follows that the NBA is relatively smooth, i.e. the energy fluctuations characterizing the roughness is comparable to  $k_B T_s$ . The roughness associated with the NBA implies that the polypeptide chain spends a finite amount of time in close proximity

$(\chi(t) \approx \langle \chi \rangle)$  to the native conformation prior to reaching it. It is worth emphasizing that this sequence ( $\sigma = 0.20$ ) fluctuates only around the native state even for  $t > \tau_{1i}$  for all the trajectories examined.

Of the nine sequences we have examined I is the fastest folder, i.e., it has the smallest folding time. Nevertheless, the partition factor  $\Phi$  is slightly (but measurably) less than unity. The amplitude of the slow component is very small (for this sequence the biexponential fit to  $P_u(t)$  suffices). These observations suggest that the underlying topography explored could be somewhat different from that of sequence G which is also a fast folder. Most of the trajectories reach the native state for sequence I rapidly without forming any intermediates and resemble the behavior shown in Fig. (5) for sequence G. However, there are "off-pathway" trajectories for this sequence an example of which is shown in Fig. (7). The inherent structures at the kinetic part for this particular trajectory ( $t < \tau_{1i}$ ) were determined using the conformations labeled (1-6) (Fig. (7)). In addition, the inherent structures were also calculated using the conformations (7-12) that the chain samples after the first passage time for this trajectory. We found that these inherent structures are all identical and differ very slightly (as measured by the overlap function). Consequently we characterize them as native-like intermediates. This sequence, although is a fast folder, has at least one competing basin of attraction (CBA) in which the structure is quite similar to the native state. Since there is a small fraction of molecules that reach the CBA prior to reaching the NBA the  $\Phi$  value is smaller than unity. The comparison between sequences G and I, both of which folds very rapidly, shows that there can be significant differences in the underlying energy surface. This is further illustrated in Sec. (IV.E).

According to our classification sequence E is at least a moderate folder and exhibits the full range of the kinetic partitioning mechanism ( $\Phi = 0.72$ ). There is a significant component of initial trajectories that reach the native state via three stage multipathway mechanism. Examples of these off-pathway trajectories are shown in Fig. (6). We have obtained the inherent structures using conformations labeled (1-6) in Fig. (6a) (that occur before  $\tau_{1i}$ ) and using the conformations labeled (7-20) (that are sampled for times greater than  $\tau_{1i}$ ).

It is found that these structures are nearly the same (excluding structure (6)) indicating that, in this instance, the polypeptide samples native-like intermediates en route the native conformation. In this sense the behavior for this trajectory is no different from that observed for off-pathway trajectories for sequence I (Fig. (7)).

The result of a similar analysis using another trajectory shown in Fig. (6b) is dramatically different. The inherent structures obtained using the conformations labeled (1) and (2) and (3-7) are completely different from each other. Furthermore, the equilibrium intermediates identified with the inherent structures obtained using the instantaneous conformations (11-17) do not resemble those calculated during the kinetic portion (1-7). We do find that the equilibrium intermediates for this trajectory (11-17) are virtually identical to those calculated using the conformations (CBA's) sampled by other trajectories displayed in Figs. (6a,8). Examination of other off-pathway trajectories reveal the presence of an exceptionally stable intermediate with  $\chi \approx 0.8$ . In fact, this intermediate survives for  $90,000\tau_L$ , while a typical first passage time is only about  $1000\tau_L$ . Such intermediates described above are never visited again after folding is completed and hence they are kinetic intermediates.

These observations imply that for moderate and slow folders there are several competing basins of attraction. Some of these serve as equilibrium intermediates, i.e., these have native-like characteristics and the chain revisits them even after reaching the native state. Others, which occur relatively early in the folding process, perhaps during the initial collapse process itself, are kinetic intermediates that are not visited after the native state is reached, at least during the time course of our simulations. Thus, for moderate and slow folders one has a distribution of CBA's. The presence of CBA's provide the entropic barriers to folding [46] resulting in slow approach to the native state. In contrast, for fast folders the only intermediates that are encountered, if at all, are all native-like. Thus, for fast folding sequences only the NBA dominates. In such cases the energy landscape can be thought of as being funnel-like [2,27].

## E. Free energy profiles

The analysis in the preceding subsection indicates that the free energy profile can be quite complex. The shapes of these profiles depend crucially on the sequence and external conditions (in our simulations that is specified only by the temperature). We have attempted a caricature of the free energy surface by computing the histogram of states expressed in terms of the potential energy  $E_p$  and  $\chi$ . The histogram of states, which measures the probability of occurrence of the state with a given  $E_p$  and  $\chi$ , is defined as

$$g(E_p, \chi) = \frac{1}{M} \sum_{i=1}^M \frac{1}{\tau_{max} - \tau_{1i}} \int_{\tau_{1i}}^{\tau_{max}} \delta(E_p - E_{p,i}(t)) \delta(\chi - \chi_i(t)) ds, \quad (30)$$

where  $E_{p,i}(t)$  and  $\chi_i(t)$  are the values of potential energy and overlap function for the trajectory  $i$  at time  $t$  averaged over a small interval of  $5\tau_L$ . We have calculated  $g(E_p, \chi)$  for three sequences at the sequence dependent simulation temperature  $T_s$ . The values of  $M = 100$ , a grid size of 0.1 is used for  $E_p$  and  $\chi$  is increased in intervals of 0.01. If  $\tau_{max} \gg \tau_{1i}$  then Eq. (30) gives the equilibrium distribution function. A free energy profile may be illustrated using the potential of mean force defined as

$$W(E_p, \chi) = -k_B T_s \ln[g(E_p, \chi)]. \quad (31)$$

In Figs. (10-12) we plot  $g(E_p, \chi)$  for the three sequences. The bottom panel in each of these figures shows the contour plot of the histogram of states. For sequence G (Fig. (10)) it is clear that the NBA is the only dominant maximum and consequently the kinetics on this surface is expected to be two state-like. The plots in Fig. (10) for sequence G also show that after the NBA is located the chain only fluctuates in the NBA. The free energy profile for sequence I (as suggested by Fig. (11)) has in addition to the NBA at least one CBA. The presence of the CBA makes  $\Phi$  smaller than that for sequence G, for which  $\Phi = 1.0$ . Proteins with a larger  $\sigma$  would have several CBA's. This is clearly indicated in Fig. (12) for sequence E which shows that there are two discernible CBA's which makes this model protein only a moderate folder. The profile of the potential of mean force for this sequence,

computed using Eq. (31), is shown in Fig. (13). This figure shows that in general one has a complex structure for the free energy profile. It is also clear that this multivalley structure naturally leads to the KPM discussed in Sec. (IV.C). These figures also show that in special cases (small values of  $\sigma$ ) the folding kinetics can be described in terms of only the NBA or folding funnel [2,27].

#### F. Dependence of $\tau_F$ on $\sigma$

It is clear from the results discussed above that the parameter  $\sigma$  (for a given external condition, which in our case is the simulation temperature) may be used to predict approximate kinetic behavior of various sequences. The folding time  $\tau_F$ , which is taken to be the mean first passage time  $\tau_{MFPT}$ , is plotted as a function of  $\sigma$  in Fig. (14a). This graph shows a remarkable correlation between these  $\tau_F$  and  $\sigma$ . The sequences with small  $\sigma \lesssim 0.4$  fold to the native conformation very rapidly, so that  $\tau_F$  is less than about  $600\tau_L$ . However,  $\tau_F$  for the sequence with largest  $\sigma = 0.65$  is as large as  $875258\tau_L$ . Thus, variation of the parameter  $\sigma$  from 0.14 to 0.65 results in three orders of magnitude increase in the folding time (from  $461\tau_L$  to  $875258\tau_L$ ). It must be noted that the correlation between  $\tau_F$  and  $\sigma$  should be considered as statistical. One can easily notice few pairs of closely located data points in Fig. (14a), for which larger value of  $\sigma$  does not correspond to larger  $\tau_F$ . Nevertheless, the general conclusion following from Fig. (14a) remains apparent: the parameter  $\sigma$  allows us to predict the trend in the folding rate of the sequences by knowing only its thermodynamic properties, such as  $T_\theta$  and  $T_F$ . It should also be pointed out that because of the difficulty in computing the low energy spectra of the off-lattice models [59,60] correlations between folding times and other quantities (such as the energy gap or the relative value of the native energy compared to that of non-native conformations) were not tested. In addition, there appears to be no unambiguous way to determine the kinetic glass transition temperature,  $T_{g,kin}$ . Therefore, we have not tested the proposal that foldable sequences have large values  $T_F/T_{g,kin}$  [53].

In order to study the dependence of the folding time on the parameter  $\sigma$  we used the function  $P_u(t)$  and defined folding time as the mean first passage time  $\tau_{MFPT}$  (see Eq. (24)). It was already mentioned above that the alternative way is to analyze the overlap function  $\langle \chi(t) \rangle$  and take the largest exponent  $\tau_2$  in the exponential fit to  $\langle \chi(t) \rangle$  as an estimate for the folding time. Due to computational limitations we did this only for five sequences and found the trend similar to that illustrated in Fig. (14a), i.e the folding time  $\tau_2$  correlates remarkably well with the parameter  $\sigma$ .

#### **G. Kinetics and folding times at moderate friction**

The results presented above have been obtained with the value of friction coefficient fixed at  $\zeta_L = 0.05$ . In order to study the dependence of the folding kinetics on  $\zeta$  we have performed the same study of nine sequences at a larger value of the friction coefficient  $\zeta_M = 5 = 100\zeta_L$ . The plot showing the folding time  $\tau_F = \tau_{MFPT}$  as a function of the parameter  $\sigma$  at  $\zeta_M$  is displayed in Fig. (14b). In accord with the results obtained at the lower value of  $\zeta_L$  this figure also unambiguously demonstrates a good correlation between  $\sigma$  and  $\tau_F$ , so that the sequences with small values of  $\sigma$  fold much faster than the sequences, having large  $\sigma$ . Specifically, the sequence labeled I, which has the smallest value of  $\sigma = 0.14$ , reaches the native conformation very rapidly within  $\tau_F = 1554\tau_L$ , while the sequence labeled A with  $\sigma = 0.65$  folds very slowly within  $\tau_F = 2.4 \times 10^6\tau_L$ . As one may expect the overall folding times in the moderate friction limit are considerably larger than in the low friction limit. The folding times vary almost linearly with  $\zeta$ . For most sequences the ratio  $\tau_F(\zeta_M)/\tau_F(\zeta_L)$  is 3 - 4. The largest value of this ratio is found for the slow folding sequence labeled D and is equal to 5.

In order to compare the folding kinetics at  $\zeta_M$  with those obtained at  $\zeta_L$  we analyzed several folding trajectories. Fig. (15) presents typical folding trajectory (in terms of the overlap function  $\chi(t)$ ) for the sequence G, which displays two state kinetics and is classified as a fast folder. This figure shows that after few tertiary native contacts are established

the chain rapidly reaches the native state. In Fig. (16) we plot  $\chi(t)$  for typical slow (upper panel) and fast (lower panel) trajectories for the sequence E, which, in contrast to sequence G, exhibits KPM and is classified as a moderate folder. It is seen that the fast trajectory for the sequence E is very similar to a typical trajectory for the sequence G. The reason for this is that the underlying mechanism for the fast process, namely NCNC mechanism, is exactly identical. It is also very important to note that similar plots for these two sequence (Figs. (5-6,8)) obtained at  $\zeta_L$  are virtually the same as those shown in Figs. (15,16). This allows us to suggest that principal mechanisms of protein folding, such KPM, nucleation collapse, appear to be independent of the viscosity of surrounding medium. The time scales and the kinetic partition factor  $\Phi$ , however, depend critically on viscosity [22].

The classification of sequences into slow and fast folders based on the parameter  $\sigma$  can also be carried out with the larger value of  $\zeta_M$ . Fast folding sequences (4 out of 9) are characterized by the values of  $\sigma \lesssim 0.4$ . The mean first passage time for fast folders  $\tau_{MFPT}$  is below  $3000\tau_L$ . The function  $P_u(t)$  for fast folders is adequately fit (apart from one sequence) with single exponential just as in the low friction limit. Thus folding of these sequences proceeds via nucleation collapse mechanism. The sequences with  $\sigma \gtrsim 0.4$  can be classified as slow or moderate folders. These sequences have significantly larger mean first passage times  $\tau_{MFPT}$  ranging from  $3285\tau_L$  to  $2.4 \times 10^6\tau_L$ . Most importantly, the fraction of unfolded molecules  $P_u(t)$  is clearly two or three exponential (see Eq. (26)) which is an apparent manifestation of KPM. As for the low friction limit the fraction of fast folding trajectories  $\Phi$  increases as the parameter  $\sigma$  decreases (Fig. (9b)). Specifically, for the sequence A ( $\sigma = 0.65$ )  $\Phi = 0.47$ , while for the fastest folding sequence I ( $\sigma = 0.14$ ) the fraction of fast trajectories becomes as large as 0.93.

## H. Quantitative dependence of $\tau_F$ on $\sigma$

It is interesting to comment on the quantitative dependence of  $\tau_F$  on  $\sigma$ . Theoretical arguments suggest that, at least at small values of  $\sigma$ ,  $\tau_F$  should scale algebraically with  $\sigma$ ,

i.e.  $\tau_F \sim \sigma^\theta$  with  $\theta = 3$  [22]. The present simulations as well as previous studies using lattice models suggest [24,48] that the data can also be fit with an exponential, i.e.

$$\tau_F \simeq \tau_0 F(N) \exp\left(\frac{\sigma}{\sigma_0}\right) \quad (32)$$

where  $\sigma_0$  depends on the value of friction and  $F(N)$  is a function that depends on  $N$ . It has been argued [22] that  $F(N) \sim N^\omega$  with  $3.8 \lesssim \omega \lesssim 4.2$  for  $\sigma \approx 0$  and  $F(N) \sim \exp(\sqrt{N})$  for larger  $\sigma$ . The data in Fig. (14) can be fit with Eq. (32) with  $\sigma_0 \approx 0.06$  at  $\zeta_L$  and  $\zeta_M$ . The fit of  $\tau_F$  to an algebraic power ( $\tau_F \sim \sigma^\theta$ ) gives  $\theta \approx 3.9$  at  $\zeta_L$  and  $\zeta_M$ . Further work will be needed to fully quantify the precise dependence of  $\tau_F$  on  $\sigma$ . It appears that both Eq. (32) and the algebraic behavior [22] account adequately for the data given here and elsewhere for lattice models. The fit given in Eq. (32) appears to be a bit more accurate.

## V. IMPLICATIONS FOR EXPERIMENTS

The results presented here together with the time scale estimates given in the Appendix have a number of implications for experiments. Here we restrict ourselves to providing some comparisons to the folding of chymotrypsin inhibitor 2 (CI2) which was probably the first protein for which a kinetic two state transition was established [20,21]. These experiments established that the kinetics for the fast phase, which corresponds to the molecules with proline residues in a trans conformation, follows a two state behavior. Furthermore the thermodynamics also displays a two state cooperative transition with the native conformation being stable by about  $7 \text{ kcal/mol}$  at  $T = 25^\circ\text{C}$ ,  $\text{pH} = 6.3$  and at zero denaturant concentration. Although not explicitly addressed here we have argued elsewhere [22] that the marginal stability (relative to other structurally unrelated conformations) of the native state of proteins satisfies

$$\Delta G \gtrsim k_B T \sqrt{N}, \quad (33)$$

where the unknown prefactor is assumed to be of the order of unity. The CI2 examined by Jackson and Fersht has 83 residues and consequently Eq. (33) gives  $\Delta G \approx 5.5 \text{ kcal/mol}$  at

$T = 25^\circ C$ . This is in fair agreement with the experimental determination. It appears that Eq. (33) is consistent with the marginal stability of proteins of varying size. The bound given above seems to be a good estimate of the stability of biomolecules [8]. We expect the scaling relation of the type given in Eq. (33) to be accurate to only within a factor of two. Given that there is inherent experimental uncertainty in determining  $\Delta G$  the agreement with the theoretical prediction within roughly 20 percent is remarkable.

The kinetics of folding of CI2 can be rationalized using the ideas developed here. The time scale for native conformation nucleation collapse according to Eq. (A5) is  $\tau_{NCNC} \approx 0.2 \text{ ms}$  using the parameters specified in the Appendix and with  $\sigma \approx 0.4$  (we have taken  $T_\theta \approx 60^\circ C$  and  $T_F \approx 37^\circ C$ ). If we assume that the folding time changes exponentially with  $\sigma$  (cf Eq. (32)) then the estimate for the nucleation collapse time changes to about 25 ms, where we have used  $\sigma_0 \approx 0.1$ . These estimates give an interval (a relatively broad one)  $0.2 \text{ ms} \lesssim \tau_{NCNC} \lesssim 25 \text{ ms}$ . Despite the uncertainties in the theoretical estimates (unknown prefactors, errors in the estimates of  $\gamma, a_0$  etc.) the estimated values of  $\tau_{NCNC}$  are within measured experimental values. The early experiments and more recent ones on CI2 and a mutant of CI2 indicate that the folding time for  $\tau_{NCNC}$  is in the range of  $(1.5 - 18) \text{ ms}$  [9,20,21,33].

The fastest folding time of 1.5 ms is found for a mutant of CI2 [56]. Our theoretical estimates show that even if the external conditions are constant and the length of the polypeptide chain is fixed  $\tau_{NCNC}$  can still be altered if  $\sigma$  (see Eq. (A5)) is altered. Since  $\sigma$  is very sensitive to sequence we suggest that the mutant of CI2 has a different value of  $\sigma$  than the wild type. This can readily explain the decrease in folding time for the mutant under otherwise similar external conditions. Further work is needed to quantify these ideas.

## VI. CONCLUSIONS

The folding of proteins is a complex kinetic process involving scenarios that are not ordinarily encountered in simple chemical reactions. This complexity arises due to the

presence of several energy scales and the polymeric nature of polypeptide chains. As a result, this complexity leads to a bewildering array of time scales that are only now beginning to be understood quantitatively in certain minimal models of proteins [22,23]. Despite this remarkable complexity it has been known from the pioneering studies of Anfinsen that the specification of the primary sequence determines the three dimensional structure of proteins, i.e. native state topology is encoded in the primary sequence. The study presented here as well as our earlier work on lattice models [24,43] have shown clearly how the kinetic accessibility is also encoded in the primary sequence itself. Our results suggest that a wide array of mechanisms that are encountered in the folding process is, remarkably enough, determined by a simple parameter expressible in terms of the properties that are intrinsic to the sequence but affected by external conditions. It appears that the two characteristic equilibrium temperatures  $T_\theta$  and  $T_F$  determine the rate at which a given sequence reaches the native conformation.  $T_\theta$  and  $T_F$  not only depend on the sequence but also can be dramatically changed by varying the external conditions such as pH, temperature etc. Thus, the mechanism for reaching the native conformation for a single domain protein can change dramatically depending on the external conditions. This implies that a protein that exhibits two state kinetics under given external conditions does not necessarily follow the same kinetics, if the ambient conditions (e.g., pH) are altered.

Our results show that generically the polypeptide chain reaches the native conformation by a kinetic partitioning mechanism (KPM). For a number of sequences studied here we have established that for given external conditions (for the computational studies it is the temperature only) a fraction of molecules  $\Phi$  reaches the native conformation directly via nucleation collapse mechanism, while the remainder follows a complex three stage multi-pathway kinetics. For both values of friction coefficient studied here this general scenario holds.

It is clear from our results that once the external conditions are specified  $\Phi$  is essentially determined by the interplay of  $T_\theta$  and  $T_F$  as embodied in Eq. (1). The folding time correlates extremely well with the dimensionless parameter  $\sigma = (T_\theta - T_F)/T_\theta$  independent of the value

of the external friction. The remarkable correlation between  $\sigma$  and several kinetic properties lends credence to the notion that in small proteins at least a single collective coordinate description of folding may suffice [54]. It also follows from this study that only when  $\sigma$  is small can folding be described in terms of NBA. For moderate and slow folders it is important to consider the interplay between NBA and CBA in determining folding kinetics. The independence of our general conclusions on the type of models (lattice versus off-lattice) [24,43] and on the details of the dynamics (Langevin dynamics or Monte Carlo) seems to indicate that the kinetic partitioning mechanism (along with  $\sigma$  determining the trends in folding times) may describe in a concise fashion the scenarios by which single domain proteins reach the native conformation.

There are quantitative differences between the results obtained for lattice and off-lattice models. For example using simulations of lattice models it was concluded that fast folders (with  $\Phi \approx 1.0$ ) have values of  $\sigma$  less than about 0.15 [43]. The off-lattice models suggest that fast folders can have  $\sigma$  as large as about 0.4. Since the estimates of  $T_\theta$  and  $T_F$  using the off-lattice simulations appear to be in better accord with experiments it is tempting to suggest that for semi-quantitative comparison with experiments it is better to use off-lattice simulations.

## ACKNOWLEDGMENTS

We are grateful to Alan Fersht for informing us of folding times for CI2 and a mutant of CI2. This work was supported in part by grants from the National Science Foundation (through grant numbers CHE93-07884 and CHE96-29845) and the Air Force Office of Scientific Research. T.V. gratefully acknowledges financial support from the Ecole Normale Supérieure de Lyon, France.

## APPENDIX A:

In this appendix we map the natural time units to real times so that an assessment of the folding times for these minimal models as well as for small sized proteins can be made. In addition using a mapping between these models and proteins estimates for folding times for proteins with small number ( $\lesssim 70$ ) of amino acids are also presented. We expect these estimates to be accurate to within an order of magnitude due to large uncertainties in the estimates of various quantities as well as a lack of theoretical understanding of the conjectures. From the equation of motion (see Eq. (11)) it is clear that when the inertial term dominates the natural unit of time is  $\tau_L = (m_0 a_0^2 / \epsilon_h)^{1/2}$ . Typical values of  $m_0$  and  $a_0$  for amino acid residues are  $3 \times 10^{-22} g$  and  $5 \times 10^{-8} cm$ , respectively. These are the masses and the Van der Waals radius of the amino acid residues. The hydrophobic interaction energy  $\epsilon_h$  is of the order of  $1 kcal/mol$  or  $7 \times 10^{-14} erg$ . If these values are changed by factor of two or so there will be not a significant change in our conclusions. Assuming that a bead in our model roughly represents one amino acid we evaluate  $\tau_L$  as

$$\tau_L = \left( \frac{m_0 a_0^2}{\epsilon_h} \right)^{1/2} \approx 3 ps. \quad (A1)$$

The value of the low friction coefficient used in our simulations  $\zeta_L = 0.05 m / \tau_L = 5 \times 10^{-12} g/s$  while the value of  $\zeta_M = 100 \zeta_L = 5 \times 10^{-10} g/s$ . It is interesting to compare these values for  $\zeta$  to that obtained in water which has at room temperature  $T = 25^\circ C$  a viscosity of  $0.01 Poise$  with  $1 Poise$  being equal to  $1 g/(s \cdot cm)$ . The friction on a bead of length  $a_0$  may be estimated as

$$\zeta_{water} \simeq 6\pi\eta_{water}a_0 \approx 9 \times 10^{-9} g/s. \quad (A2)$$

From this we get  $\zeta_L / \zeta_{water} \approx 10^{-3}$ , while  $\zeta_M / \zeta_{water} \approx 0.1$ . The low friction would correspond to the energy diffusion regime in the Kramer's description of the unfolding to folding reaction. In the moderate friction there could be a competition between inertial and viscous damping terms leading perhaps to the Kramer's turnover regime familiar in the literature on simple reactions.

In the overdamped limit the inertial term can be ignored and the natural measure for time is

$$\tau_H \simeq \frac{\zeta a^2}{k_B T_s} \simeq \frac{6\pi\eta a^3}{k_B T_s} = \alpha \tau_L \frac{\epsilon_h}{k_B T_s}, \quad (\text{A3})$$

where  $\alpha$  is a constant. In our simulations  $\alpha = 0.05$  for  $\zeta_L$  and  $\alpha = 5.0$  for  $\zeta_M$ . The typical value of  $\epsilon_h/k_B T_s$  is about 2, where once again we have used  $\epsilon_h = 1\text{kcal/mole}$  and taken  $T_s$  to be the room temperature. For water at room temperature  $\tau_H \approx 3\text{ns}$  with  $\alpha \approx 100$ . If we assume that the higher value of friction used in this study is in the slightly overdamped limit then the approximate time unit becomes  $\tau_M \approx 0.3\text{ns}$ . Since the higher value of friction is more realistic we can estimate the folding times for small proteins using the computed time scale. For  $\alpha = 5.0$  our simulation results give the folding time ranging from  $100 \tau_M$  to  $10^6 \tau_M$ . The folding time for the case of higher friction (with  $\alpha$  exceeding 5) also ranges from  $10^3 \tau_M$  (for the smallest  $\sigma$ ) to  $10^6 \tau_M$  (for the largest  $\sigma$ ) (Klimov and Thirumalai, unpublished). A naive estimate using these results would suggest that the folding time for these sequences ranges from  $10^{-6}\text{s}$  to  $10^{-4}\text{s}$ .

A better estimate of these times can perhaps be made by recognizing that each bead in the minimal model corresponds to a blob containing  $g$  number of amino acids [42]. If the structure within a blob is represented by roughly spherical size  $a$  than we can use  $a \approx g^\nu a_0$ , where  $g^\nu$  is the "swelling factor" mapping the minimal model to real proteins. Then the natural time unit for the motion of such a blob in the overdamped limit becomes

$$\tau_H^R \simeq \frac{6\pi\eta g^{3\nu} a_0^3}{k_B T} = g^{3\nu} \tau_H \quad (\text{A4})$$

The range of  $\nu$  is  $\frac{1}{3} - 1$ , with  $\nu = \frac{1}{3}$  corresponding to globular structure within a blob and  $\nu = 1$  corresponding to maximum repulsion among the residues in a blob. This should be viewed as a guess and is not expected to be correct given that  $g$  is small. Realistic values of  $g$  are expected to be between 2 and 3 [23,55] making the 22-mer minimal model to (perhaps) correspond with 44-66 amino acid residue proteins. For  $g = 2$ ,  $\tau_H^R$  ranges from  $0.4\text{ns}$  to  $1.6\text{ns}$ , while for  $g = 3$   $\tau_H^R$  ranges from  $0.4\text{ns}$  to  $5.4\text{ns}$ . Assuming that  $g = 3$  and  $\nu = 1$

(which would give the largest time scales ) the folding estimates for small proteins (number of amino acids smaller than 70) range from  $8 \times 10^{-6}s$  (for small  $\sigma$ ) to  $10ms$  (for large  $\sigma$ ).

This exercise suggests that no matter how the mapping is done the most relevant time scale for folding kinetics of small proteins under normal folding conditions (around room temperature and low denaturant concentration) is between microseconds to milliseconds. In particular, for those proteins that reach the native conformation predominantly via the nucleation collapse process (characterized by relatively small  $\sigma$ ) the time scale for folding is between microseconds to milliseconds for small proteins. One of us has argued [22] that the time scale for the NCNC process is given by

$$\tau_{NCNC} \simeq \frac{\eta a_0}{\gamma} \sigma^3 N^\omega \quad (A5)$$

where  $\omega$  is in the range of 3.8 to 4.2. There is usually a large uncertainty in the surface tension  $\gamma$  between the hydrophobic residues and water. The range for  $\gamma$  is between  $25 - 75 \text{ cal}/(\text{\AA}^2 \cdot \text{mol})$ . The largest time scale to Eq. (A5) emerges when  $w \simeq 4.2$  and  $\gamma \simeq 25 \text{ cal}/(\text{\AA}^2 \cdot \text{mol})$ . Using  $\eta \simeq 0.01 \text{ Poise}$ ,  $\sigma \approx 0.2$ , and  $a_0 \approx 5 \times 10^{-8} \text{ cm}$   $\tau_{NCNC}$  ranges from  $10^{-6}s$  to  $0.1ms$  as  $N$  varies from 22 to 66. The values based on theoretical arguments (cf. Eq. (A5)) are consistent with the numerical estimates based on the simulations.

It is interesting to compare the estimates for the fast process, corresponding to the NCNC mechanism, obtained using Eqs. (A5,A4) and simulation results with experimental results. All the theoretical estimates yield  $\tau_{NCNC} \approx 0.1 \text{ ms}$ . The recent experiments on chymotrypsin inhibitor 2 suggest that the time scale for the nucleation collapse process is in the range of  $1.5 - 15 \text{ ms}$  [56] depending on external conditions. The experimental times are not inconsistent with our simulation results and theoretical estimates given the uncertainty in the values of the various parameters. Our studies further underscore the importance of processes relevant for folding of proteins in submillisecond time scale especially for the NCNC process. Further experiments on these time scales are needed for an explicit experimental demonstration of the native conformation nucleation collapse mechanism [61–63].

## REFERENCES

[1] Dill, K.A., Bromberg, S., Yue, K., Fiebig, K.M., Yee, D.P., Thomas, P.D. & Chan, H.S. (1995). Principles of protein folding - A perspective from simple exact models. *Protein Sci.* **4**, 561-602.

[2] Bryngelson, J.D., Onuchic, J.N., Socci, N.D. & Wolynes, P.G. (1995). Funnels, pathways and the energy landscape of protein folding: A synthesis. *Proteins Struct. Funct. Genet.* **21**, 167-195.

[3] Wolynes, P.G., Onuchic, J.N. & Thirumalai, D. (1995). Navigating the folding routes. *Science* **267**, 1619-1620.

[4] Chan, H.S. & Dill, K.A. (1994). Transition states and folding dynamics of proteins and heteropolymers. *J. Chem. Phys.* **100**, 9238-9257.

[5] Thirumalai, D. (1994) Theoretical perspectives on in vitro and in vivo protein folding. In: *Statistical Mechanics, Protein Structure, and Protein Substrate Interactions*. (Doniach, S., ed.), pp. 115-133, Plenum Press, New York.

[6] Abkevich, V.I., Gutin, A.M. & Shakhnovich, E. (1994). Specific nucleus as the transition state for protein folding: Evidence from the lattice model. *Biochemistry* **33**, 10026-10036.

[7] Socci, N.D. & Onuchic, J.N. (1995). Kinetic and thermodynamic analysis of protein-like heteropolymers: Monte Carlo histogram technique. *J. Chem. Phys.* **103**, 4732-4744.

[8] Thirumalai, D. & Woodson, S.A. (1996). Kinetics of folding of proteins and RNA. *Acc. Chem. Res.* (to be published).

[9] Otzen, D.E., Itzhaki, L.S. & Fersht, A.R. (1994). Structure of the transition state for the folding/unfolding of the barley chymotrypsin inhibitor 2 and its implications for mechanisms of protein folding. *Proc. Natl. Acad. Sci. USA* **91**, 10422-10425.

[10] Fersht, A.R. (1995). Optimization of rates of protein folding: The nucleation - condensation mechanism and its implications. *Proc. Natl. Acad. Sci. USA* **92**, 10869-10873.

[11] Radford, S.E. & Dobson, C.M. (1995). Insights into protein folding using physical techniques: Studies of lysozyme and alpha-lactalbumin. *Phil. Trans. Roy. Soc. Lond. B* **348**, 17-25.

[12] Sosnick, T. R., Mayne, L., Hiller, R. & Englander, S. W. (1994). The barriers in protein folding. *Nature Struct. Biol.* **1**, 149-156.

[13] Schindler, T., Herrler, M., Marahiel, M.A. & Schmid, F.X. (1995). Extremely rapid folding in the absence of intermediates. *Nature Struct. Biol.* **2**, 663-673.

[14] Kieffhaber, T. Kinetic traps in lysozyme folding. (1995). *Proc. Natl. Acad. Sci. USA* **92**, 9029-9033.

[15] Guo, Z. & Thirumalai, D. (1995). Kinetics of protein folding: Nucleation mechanism, time scales, and pathways. *Biopolymers* **36**, 83-103.

[16] Thirumalai, D. & Guo, Z. (1995). Nucleation mechanism for protein folding and theoretical predictions for hydrogen-exchange labeling experiments. *Biopolymers* **35**, 137-140.

[17] Camacho, C.J. & Thirumalai, D. (1995). Theoretical predictions of folding pathways using the proximity rule with applications to BPTI. *Proc. Natl. Acad. Sci. USA* **92**, 1277-1281.

[18] Dadlez, M. & Kim, P.S. (1995). A third native one-disulphide intermediate in the folding of bovine pancreatic trypsin inhibitor. *Nature Struct. Biol.* **2**, 674-679.

[19] Mirny, L.A., Abkevich, V. & Shakhnovich, E.I. (1996). Universality and diversity of the protein folding scenarios: a comprehensive analysis with the aid of a lattice model. *Folding & Design* **1**, 103-116.

[20] Jackson, S.E. & Fersht, A.R. (1991). Folding of chymotrypsin inhibitor 2. 1. Evidence

for a two-state transition. *Biochemistry* **30**, 10428-10435.

[21] Jackson, S.E. & Fersht, A.R. (1991). Folding of chymotrypsin inhibitor 2. 2. Influence of proline isomerization on the folding kinetics and thermodynamic characterization of the transition state of folding. *Biochemistry* **30**, 10436-10443.

[22] Thirumalai, D. (1995). From minimal models to real proteins: Time scales for protein folding kinetics. *J. Physique (Paris) I* **5**, 1457-1467.

[23] Onuchic, J.N., Wolynes, P.G., Luthey-Schulten, Z.A. & Soccia, N.D. (1995). Toward an outline of the topography of a realistic protein-folding funnel. *Proc. Natl. Acad. Sci. USA* **92**, 3626-3630.

[24] Klimov, D.K. & Thirumalai, D. (1996). A Criterion that determines the foldability of proteins. *Phys. Rev. Lett.* **76**, 4070-4073.

[25] Camacho, C.J. & Thirumalai, D. (1993). Kinetics and thermodynamics of folding in model proteins. *Proc. Natl. Acad. Sci. USA* **90**, 6369-6372.

[26] Alexander, P., Fahnstock, S., Lee, T., Orban, J. & Bryan, P. (1992). Thermodynamic analysis of the folding of the streptococcal protein G IgG-binding domains B1 and B2: Why small proteins tend to have high denaturation temperatures. *Biopolymers* **31**, 3597-3603.

[27] Leopold, P.E., Montal, M. & Onuchic, J.N. (1992). Protein folding funnels: A kinetic approach to the sequence-structure relationship. *Proc. Natl. Acad. Sci. USA* **89**, 8721-8725.

[28] Honig, B. & Cohen, F.E. (1996). Adding backbone to protein folding: Why protein are polypeptides. *Folding & Design* **1**, R17-R20.

[29] Rey, A. & Skolnick, J. (1991). A comparison of lattice Monte Carlo dynamics and Brownian dynamics folding pathways of  $\alpha$ -helical hairpins. *Chem. Phys.* **158**, 199-219.

[30] Garrett, D. G., Kastella, K. & Ferguson, D. M. (1992). New results on protein folding from simulated annealing. *J. Am. Chem. Soc.* **114**, 6555-6556.

[31] Guo, Z. & Thirumalai, D. (1996). Kinetics and thermodynamics of folding of a *de novo* designed four-helix bundle protein. *J. Mol. Biol.* **263**, 000-000 (to be published).

[32] Straub, J. E. & Thirumalai, D. (1996). On the approximate incorporation of side chains in the minimal off-lattice models of proteins (unpublished).

[33] Itzhaki, L.S., Otzen, D.E. & Fersht, A.R. (1995). The structure of the transition state for folding of chymotrypsin inhibitor 2 analyzed by protein engineering methods: Evidence for a nucleation-condensation mechanism for protein folding. *J. Mol. Biol.* **254**, 260-288.

[34] Sosnick, T.R., Mayne, L. & Englander, S.W. (1996). Molecular collapse: The rate limiting step in two-state cytochrome C folding. *Proteins Struct. Funct. Genet.* (to be published).

[35] Honeycutt, J.D. & Thirumalai, D. (1992). The nature of folded states of globular proteins. *Biopolymers* **32**, 695-709.

[36] Pangali, C., Rao, M. & Berne, B.J. (1979). A Monte Carlo simulation of the hydrophobic interaction. *J. Chem. Phys.* **71**, 2975-2981.

[37] Andersen, H.C. (1983). Rattle: A "velocity" version of the shake algorithm for molecular dynamics calculations. *J. Comp. Phys.* **52**, 24-34.

[38] Creighton, T.E. (1993). *Proteins: Structures and Molecular Properties*, W.H. Freeman & Co., New York.

[39] McCammon, J.A. & Harvey, S.C. (1988). *Dynamics of Proteins and Nucleic Acids*, Cambridge University Press, Cambridge.

[40] Swope, W.C., Andersen, H.C., Berens, P.H. & Wilson, K.R. (1982). A computer simulation method for the calculation of equilibrium constants for the formation of physical

clusters of molecules: Application to small water clusters. *J. Chem. Phys.* **76**, 637-649.

[41] Amara, P. & Straub, J.E. (1995). Folding model proteins using kinetic and thermodynamic annealing of the classical density distribution. *J. Phys. Chem.* **99**, 14840-14853.

[42] De Gennes, P.G. (1979). *Scaling Concept in Polymer Physics*, Cornell University Press, New York.

[43] Klimov, D.K. & Thirumalai, D. (1996). Factors governing the foldability of proteins. *Proteins Struct. Funct. Genet.* (to be published).

[44] Straub, J. & Thirumalai, D. (1993). Theoretical probes of conformational fluctuations in S-peptide and RNase A/3'-UMP enzyme product complex. *Proteins Struct. Funct. Genet.* **15**, 360-373.

[45] Bryngelson, J.D. & Wolynes, P.G. (1989). Intermediates and barrier crossing in a random energy model (with application to protein folding). *J. Phys. Chem.* **93**, 6902-6915.

[46] Camacho, C.J. & Thirumalai, D. (1995). Modeling the role of disulfide bonds in protein folding: Entropic barriers and pathways. *Proteins Struct. Funct. Genet.* **22**, 27-40.

[47] Sali, A., Shakhnovich, E. & Karplus, M. (1994). Kinetics of protein folding: A lattice model study of the requirements for folding to the native state. *J. Mol. Biol.* **235**, 1614-1636.

[48] Camacho, C.J. & Thirumalai, D. (1996). A criterion that determines fast folding of proteins: A model study. *Europys. Lett.* (to be published).

[49] Shakhnovich, E. & Gutin, A.M. (1993). A new approach to the design of stable proteins. *Protein Eng.* **6**, 793-800.

[50] Shakhnovich, E. (1994). Proteins with selected sequences fold into unique native conformation. *Phys. Rev. Lett.* **72**, 3907-3910.

[51] Deutsch, J.M. & Kurosky, T. (1996). New algorithm for protein design. *Phys. Rev. Lett.*

**76**, 323-326.

[52] Garel, T., Orland, H. & Thirumalai, D. (1996). Analytical theories of protein folding. In: *New Development in Theoretical Studies of Proteins*. (Elber, R., ed.), World Scientific, Singapore.

[53] Goldstein, R.A., Luthey-Schulten, Z.A. & Wolynes, P.G. (1992). Optimal protein-folding codes from spin-glass theory. *Proc. Natl. Acad. Sci. USA* **89**, 4918-4922.

[54] Socci, N.D., Onuchic, J.N. & Wolynes, P.G. (1996). Diffusive dynamics of the reaction coordinate for protein folding funnels. *J. Chem. Phys.* **104**, 5860-5871.

[55] Bryngelson, J.D. (1996). In: *Physics of Biological Systems*. (Flyvberg, H., ed.), Springer Verlag, New York (to be published).

[56] Otzen, D.E. & Fersht, A.R. (unpublished).

[57] Go, N. (1983). Theoretical studies of protein folding. *Ann. Rev. Biophys. Bioeng.* **12**, 183-210.

[58] Stillinger, F.H. & Weber, T.A. (1982). Hidden structure in liquids. *Phys. Rev. A* **25**, 978-989.

[59] Honeycutt, J.D. & Thirumalai, D. (1990). Metastability of the folded states of globular proteins. *Proc. Natl. Acad. Sci. USA* **87**, 3526-3529.

[60] Fukugita, M., Lancaster, D. & Mitchard, M.G. (1996). *Biopolymers* (to be published).

[61] Jones, C.M., *et al.*, & Eaton, W.A. (1993). Fast events in protein folding initiated by nanosecond laser photolysis. *Proc. Natl. Acad. Sci. USA* **90**, 11860-11864.

[62] Ballew, R.M., Sabelko, J., & Gruebele, M. (1996). Direct observation of fast protein folding: The initial collapse of apomyoglobin. *Proc. Natl. Acad. Sci. USA* **93**, 5759-5764.

[63] Pascher, T., Chesick, J.P., Winkler, J.R., & Gray, H.R. (1996). Protein folding triggered by electron transfer. *Science* **271**, 1558-1560.

## FIGURE CAPTIONS

Fig. 1. The  $\beta$ -type native structure of the sequence  $LB_9(NL)_2NBLB_3LB$  labeled G. In the turn region chain backbone adopts *gache*-conformations. The hydrophobic beads are given by a blue color, the hydrophilic beads are represented by red, and the neutral beads are shown in grey.

Fig. 2. The temperature dependence of the thermodynamic quantities for sequence G calculated using slow-cooling method: (a) overlap function  $\langle \chi(T) \rangle$ ; (b) fluctuations of the overlap function  $\Delta\chi(T)$ ; (c) energy  $\langle E(T) \rangle$ ; (d) specific heat  $C_v(T)$ . The peaks in the graphs of  $\Delta\chi(T)$  and  $C_v(T)$  correspond to the folding transition and collapse transition temperatures,  $T_F$  and  $T_\theta$ .

Fig. 3. The dependence of the simulation temperature  $T_s$ , as defined by Eq. (21), on the parameter  $\sigma = (T_\theta - T_F)/T_\theta$ .

Fig. 4. The fraction of the unfolded molecules  $P_u(t)$  as a function of time for the sequences G (a) and A (b). Time is measured in the units of  $\tau_L$  (cf. Eq. (A1)). The solid line in Fig. (4a) is a single exponential fit to the data. This implies that for this sequence folding is kinetically a two state process ( $\Phi = 1.0$ ). The solid line in Fig. (4b) is a three exponential fit to the data. The multiexponential process is indicative of the kinetic partitioning mechanism with  $\Phi = 0.43$  (see Eq. (26)).

Fig. 5. Dynamics of a typical fast-folding trajectory as measured by  $\chi(t)$  (sequence G) at  $\zeta_L$ . It is seen in Fig. (5a) that on a very short time  $380\tau_L$  the native conformation is reached. After the native conformation is reached  $\chi(t)$  fluctuates around the equilibrium value  $\langle \chi \rangle$ . (b) Another trajectory for this sequence, for which inherent structures at the times (1-6) were determined. Horizontal arrow in this plot indicates the region of native basin of attraction (NBA). It is seen that the chain approaches NBA but spends finite amount of time there before reaching the native state at  $1525\tau_L$ . Dashed line indicates  $\langle \chi \rangle = 0.26$  at  $T_s$ . Vertical arrows indicates the first passage time.

Fig. 6. Examples of two trajectories that reach the native conformation by an indirect off-pathway process. These trajectories are for sequence E at  $\zeta_L$ . The kinetics exhibited by the

off-pathway process suggests that the native state is reached by a three state multipathway mechanism. Fig. (6a) shows that after initial rapid collapse on the time scale of  $(100-200)\tau_L$  the chain gets trapped in misfolded compact structure (indicated by nearly constant value of  $\chi$  for long times). In this case the native state is eventually reached at  $\approx 3026\tau_L$ . Fig. (6b) which is given for a different slow trajectory shows that the chain samples at least two distinct misfolded structures before the first passage time is attained at  $\approx 1970\tau_L$ . In both figures numbers indicate the points where inherent structures were determined. The time course of  $\chi(t)$  reveals that the chain samples a number of kinetic and equilibrium intermediates. It was found that inherent structures (1-5,7-20) (Fig. (6a)), (11-17) (Fig. (6b)), and (1-5) (Fig. (8)) are almost identical and are accessible *before* and *after* first passage time. For this they are classified as native-like equilibrium intermediates. However, the inherent structures (1-2) and (3-7) (Fig. (6b)) are examples of kinetic intermediates. Dashed lines in these plots indicate the equilibrium value of  $\langle \chi \rangle = 0.26$  at  $T_s$ . Horizontal arrows indicate the regions of CBA's. Vertical arrows indicate the first passage time.

Fig. 7. Dynamics of one of the few off-pathway trajectories for sequence I ( $\Phi = 0.95$ ). Inherent structures are determined at the points marked by the numbers. Analysis shows that structures (1-6) and (7-12) are identical that allows us to refer to them as equilibrium native-like intermediates. Note that the vast majority ( $\approx 0.95$ ) of trajectories fold via NCNC mechanism. The native state is reached at  $2384\tau_L$ . Horizontal arrows indicate the regions of CBA's. Vertical arrow indicates the first passage time.

Fig. 8. This figure shows the dynamics of  $\chi(t)$  for one trajectory for sequence E (with  $\Phi = 0.72$ ) that reaches the native conformation rapidly. In this example the native conformation is attained at  $\approx 325\tau_L$ . Comparison of this figure with Fig. (5) (for sequence G with  $\Phi > 0.9$ ) shows that the dynamics is very similar. This implies that the underlying mechanism (NCNC mechanism) of fast folding trajectories of sequences with large  $\sigma$  (or equivalently small  $\Phi$ ) is similar to that by which the molecules reach the native state in kinetically two state manner. Horizontal arrow indicates the regions of CBA's. Vertical arrow indicates the first passage time.

Fig. 9. Correlation between the fraction of fast folding trajectories  $\Phi$  and the parameter  $\sigma = (T_\theta - T_F)/T_\theta$ . Most sequences with small  $\sigma$  have  $\Phi \approx 1.0$ . Vertical dashed line shows classification of sequences with respect to  $\Phi$ . (a) is for low friction value. (b) corresponds to moderate friction. These sequences with  $\Phi \gtrsim 0.9$  are classified as fast folders. The classification of sequences into slow category is somewhat arbitrary. The classification does not seem to depend on the value of  $\zeta$ .

Fig. 10. (a) Histogram of states  $g$  as a function of two variables,  $E_p$  and  $\chi$ , is given for sequence G. (b) The contour plot of the histogram of states  $g$  for this sequence. Lighter areas correspond to peaks of  $g$ . Single peak of the histogram of states suggests that at equilibrium the chain is completely confined to a native basin of attraction.

Fig. 11. Histogram of states  $g$  and contour plot of  $g$  for sequence I. These plots reveal two peaks of the histogram of states that manifests the presence of competing basin of attraction which makes the partition factor  $\Phi$  less than unity.

Fig. 12. Histogram of states  $g$  and contour plot of  $g$  for sequence E. One can clearly see at least three maximums of  $g$ . These plots illustrates the existence of several competing basins of attractions (intermediates) that gives rise to complex folding kinetics which features a combination of three stage multipathway and nucleation collapse mechanisms.

Fig. 13. The profile of the potential of the mean force  $W$  in terms of two variables,  $E_p$  and  $\chi$ , for sequence E. This further illustrates that the free energy landscape of this sequence features multiple funnels (basins of attractions). The plane at  $W = 3.8$  is given for eye reference.

Fig. 14. Dependence of the folding time  $\tau_F$  on the parameter  $\sigma = (T_\theta - T_F)/T_\theta$ . It is seen that  $\tau_F$  correlate remarkably well with  $\sigma$ , so that sequences with small value of  $\sigma$  reach native state very rapidly, whereas those characterized by large  $\sigma$  fold slowly. Solid lines indicate exponential fit to the data. The actual fit to the data is discussed in the text. Fig. (14a) is for the low friction value and Fig. (14b) shows data for the moderate friction limit.

Fig. 15. An example of a fast folding trajectory that reaches the native conformation by a NCNC process. This is for sequence G at  $\zeta_M$ . This figure shows that the dynamics of

the fast folding trajectory is qualitatively similar to that obtained at  $\zeta_L$  (see Fig. (5)). In both cases the native conformation is reached rapidly following the formation of a critical number of contacts (nucleus) and collapse. The first passage time for this trajectory is  $603\tau_L$ . Dashed line gives the equilibrium value of  $\langle \chi \rangle = 0.26$  at  $T_s$ . Vertical arrow indicates the first passage time.

Fig. 16. (a) An example of a slow folding trajectory as recorded by  $\chi(t)$  (sequence E) at  $\zeta_M$ . After initial rapid collapse on the time scale  $\lesssim 1000\tau_L$  the chain samples various compact conformations and finally reaches the native state at  $12919\tau_L$  as indicated by an arrow. This trajectory shows that at least four distinct kinetic structures are sampled as the chain navigates to the native conformation. Dashed line in both panels indicates the equilibrium value of  $\langle \chi \rangle = 0.26$  at  $T_s$ . (b) Typical fast folding trajectory for this sequence. This trajectory is similar to those characteristic of fast folders (see Fig. (15)). The native conformation is found very rapidly at  $563\tau_L$  as indicated by an arrow. The results displayed in Figs. (5-8) and Figs. (15,16) show that the qualitative aspect of the kinetic partitioning mechanism is not dependent on the friction coefficient. Vertical arrow indicates the first passage time.

## TABLES

TABLE I. The list of sequences and their parameters studied in simulations

| Sequence label | Sequence                   | $\Lambda$ | $T_F$ | $T_\theta$ | $\sigma$ |
|----------------|----------------------------|-----------|-------|------------|----------|
| A              | $B_9N_3(LB)_5$             | 0         | 0.20  | 0.58       | 0.65     |
| B              | $B_8(NL)_2NBLB_3(LB)_2$    | 0         | 0.30  | 0.62       | 0.51     |
| C              | $B_8NLN_2LBLB_3(LB)_2$     | 0.3       | 0.38  | 0.72       | 0.47     |
| D              | $B_9N_2LNB(LB)_4$          | 0.17      | 0.36  | 0.62       | 0.41     |
| E              | $LB_7NBNLN(BL)_2B_3LB$     | 0.1       | 0.40  | 0.66       | 0.39     |
| F              | $LB_9(NL)_2NBLB_3LB$       | 0.3       | 0.46  | 0.76       | 0.39     |
| G              | $LB_9(NL)_2NBLB_3LB$       | 0.3       | 0.62  | 0.78       | 0.20     |
| H              | $LB_9(NL)_2NBLB_3LB$       | 0.3       | 0.59  | 0.80       | 0.26     |
| I              | $LBNB_3LB_3N_2B_2LBLB_3LB$ | 0.3       | 0.54  | 0.62       | 0.14     |

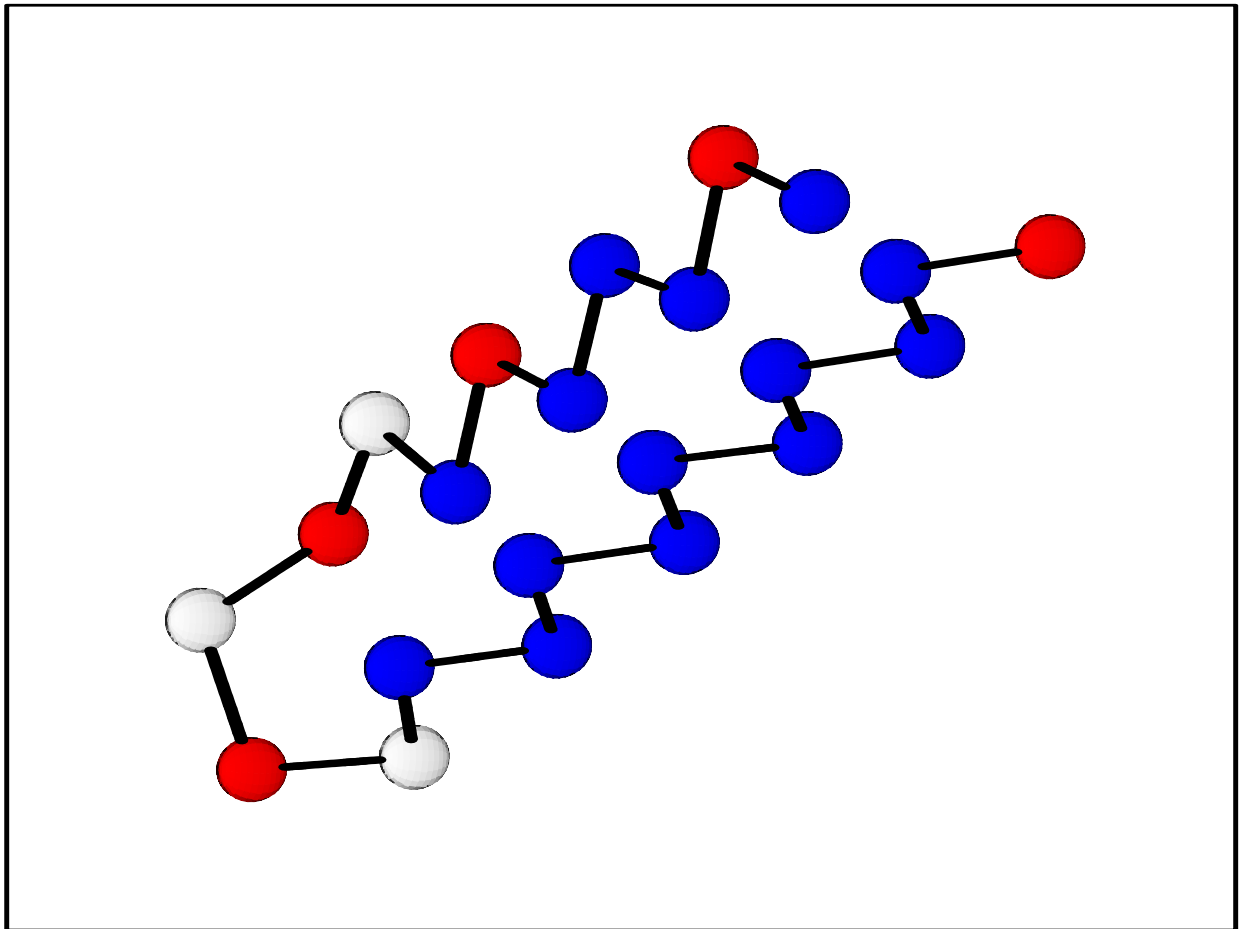


Fig. 1

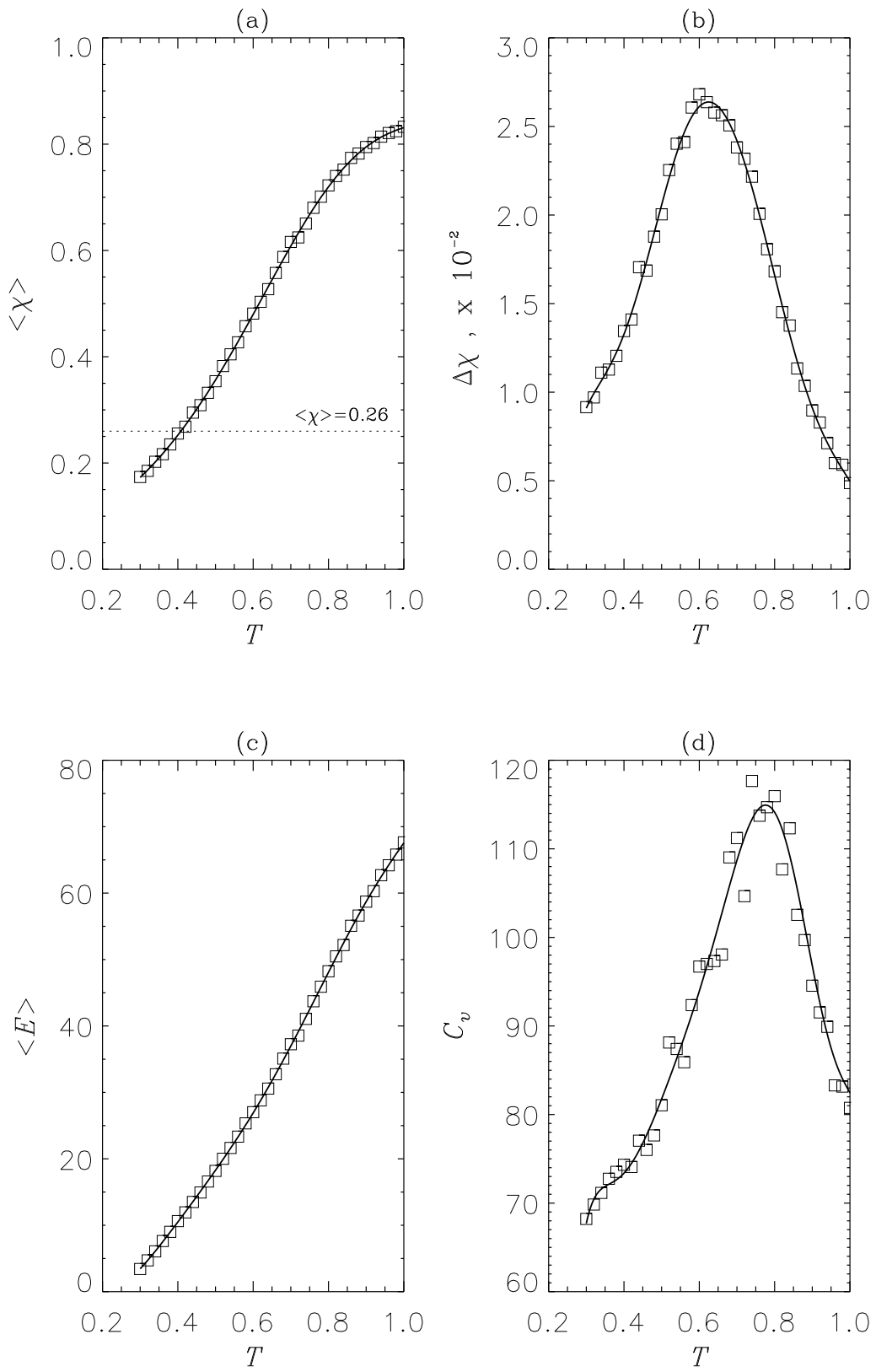


Fig. 2

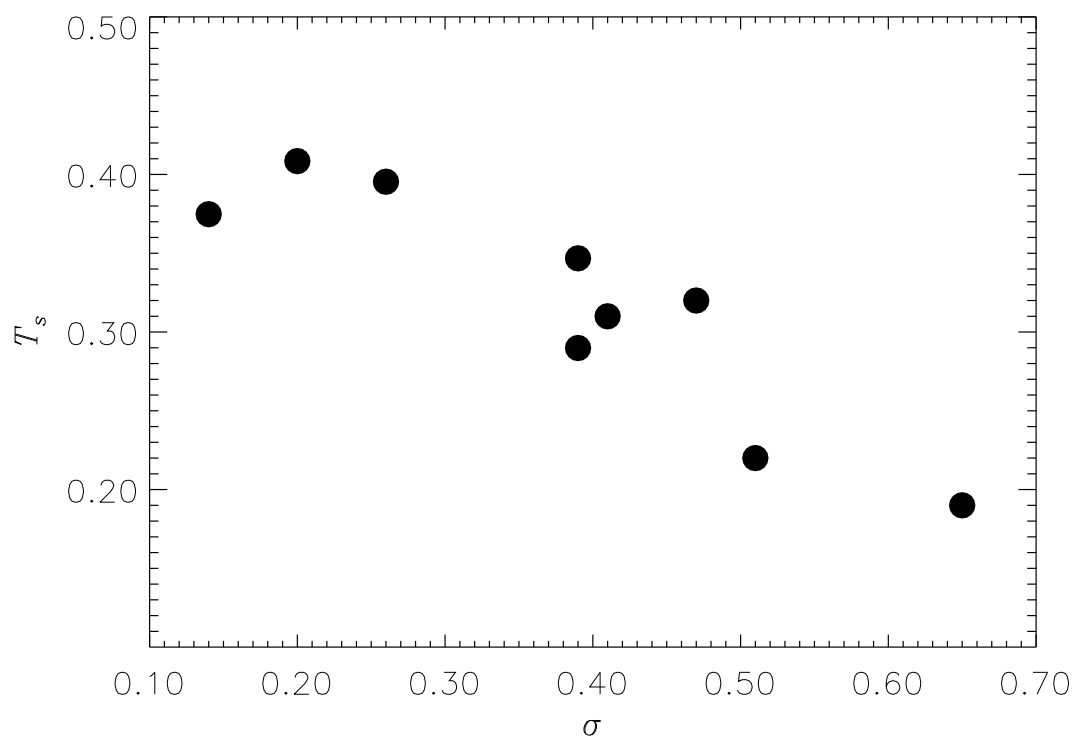


Fig. 3

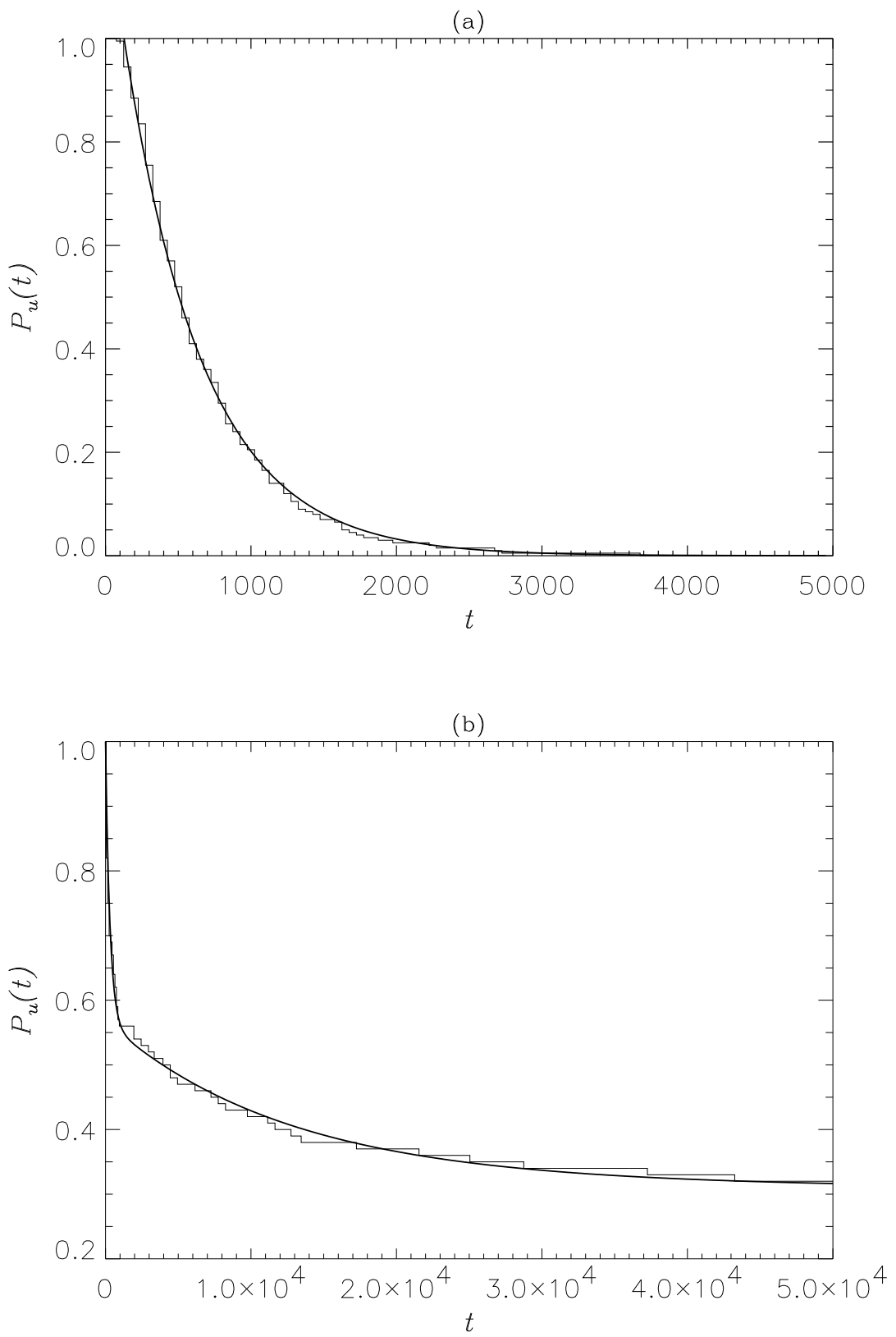


Fig. 4

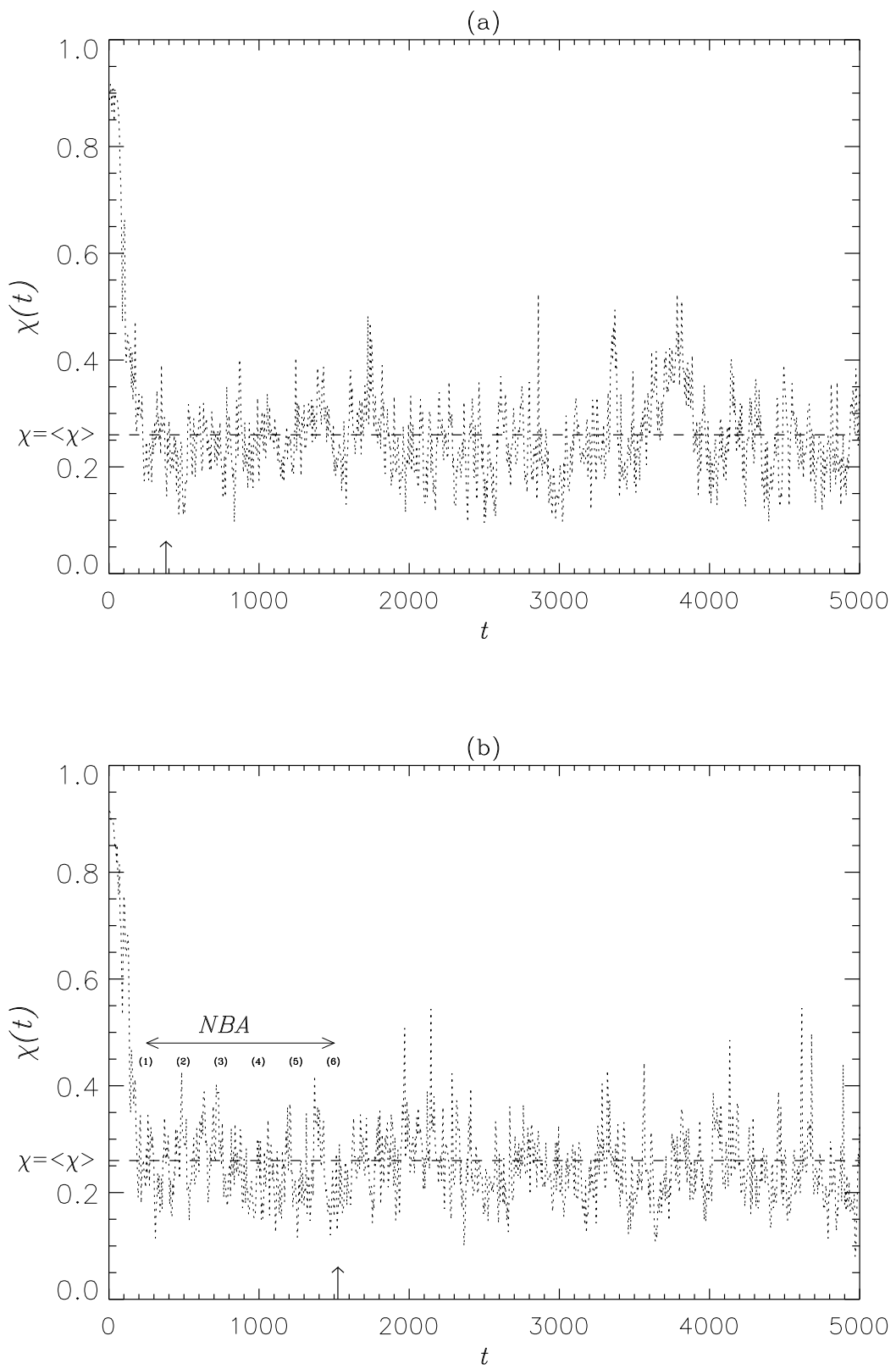


Fig. 5

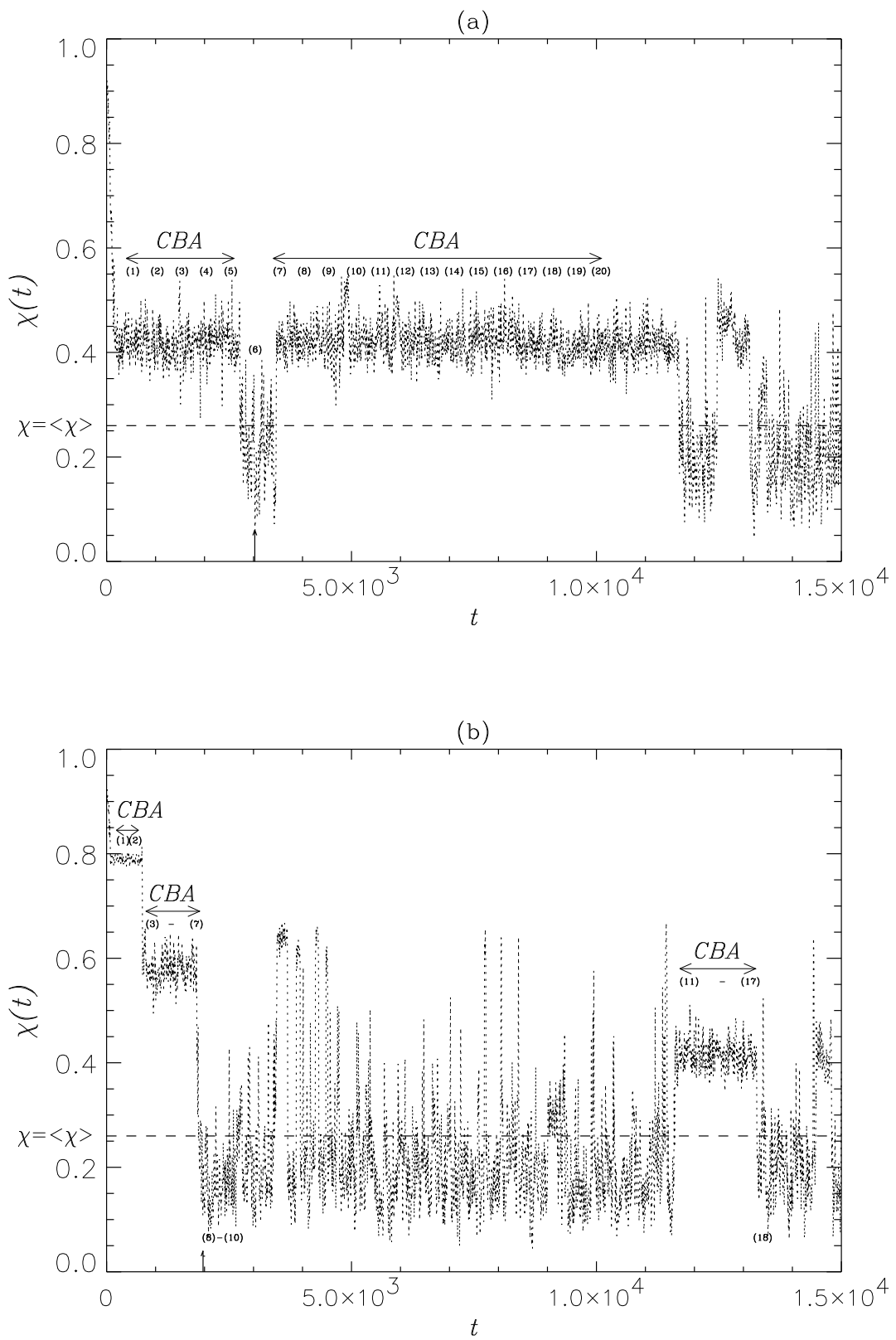


Fig. 6

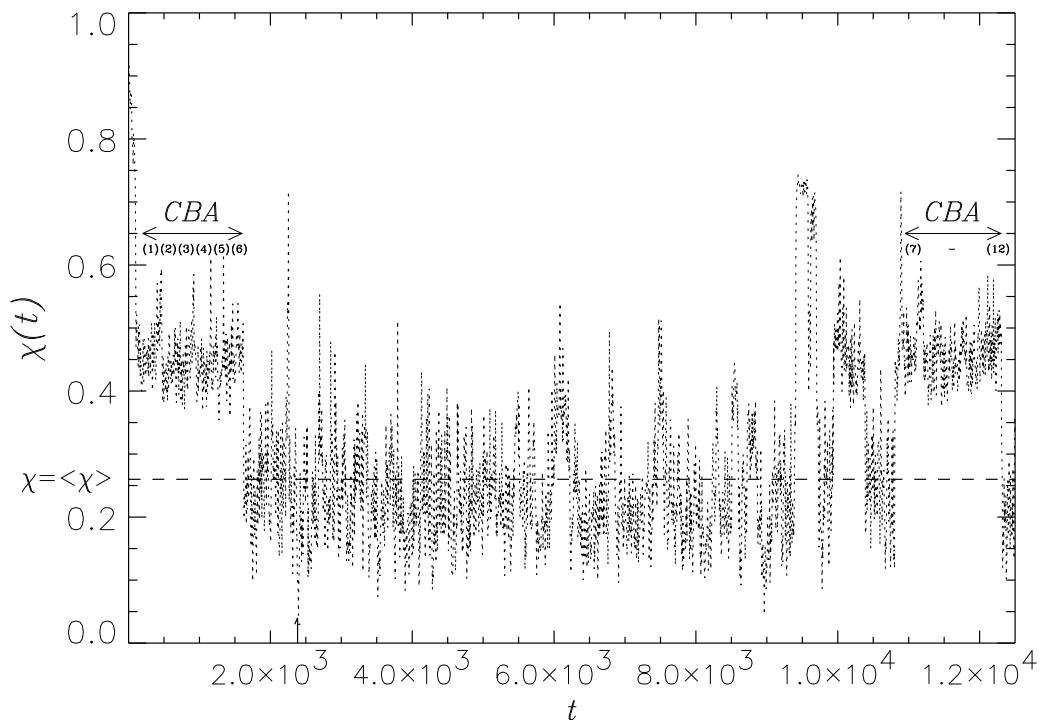


Fig. 7

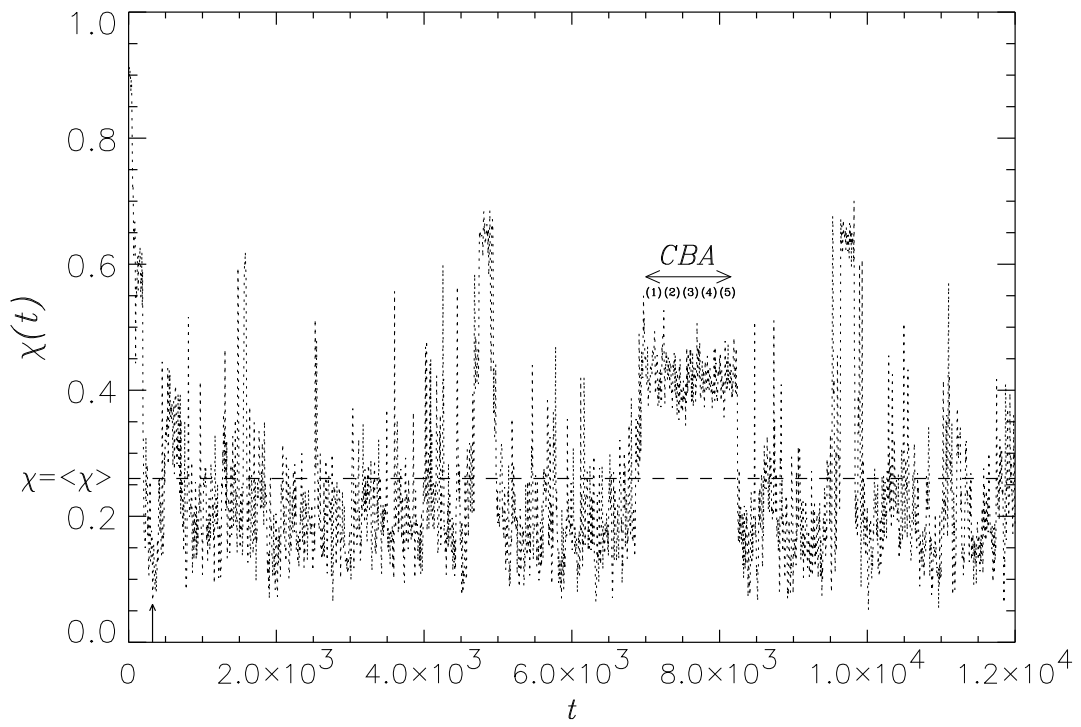


Fig. 8

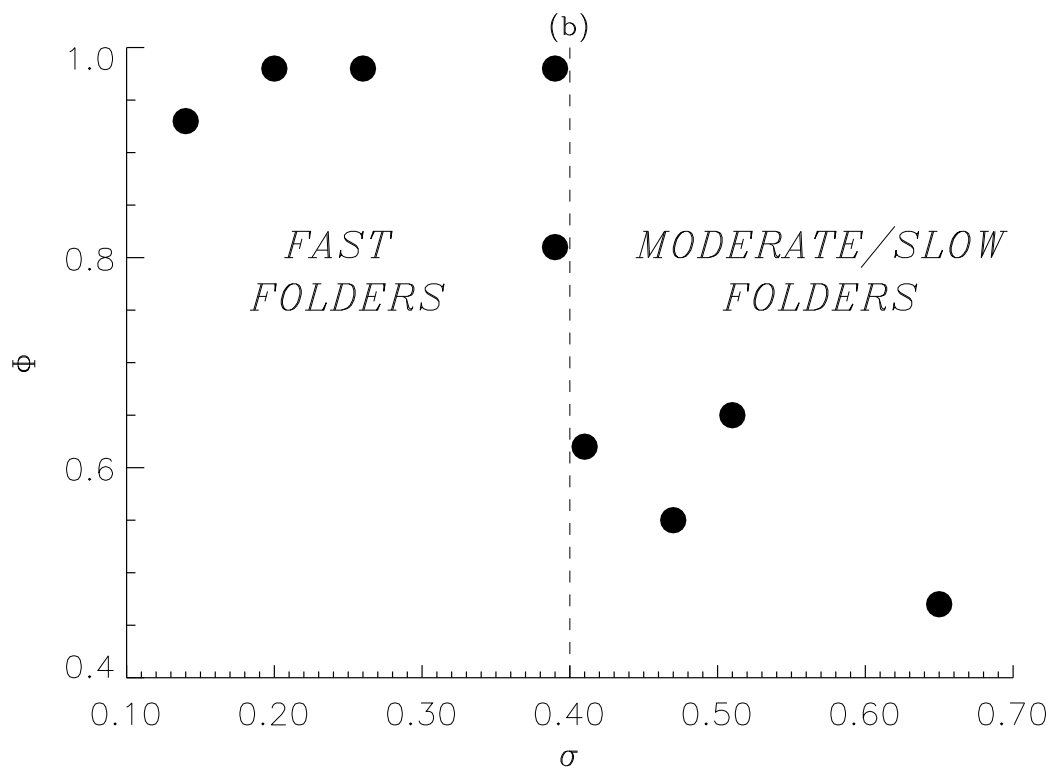
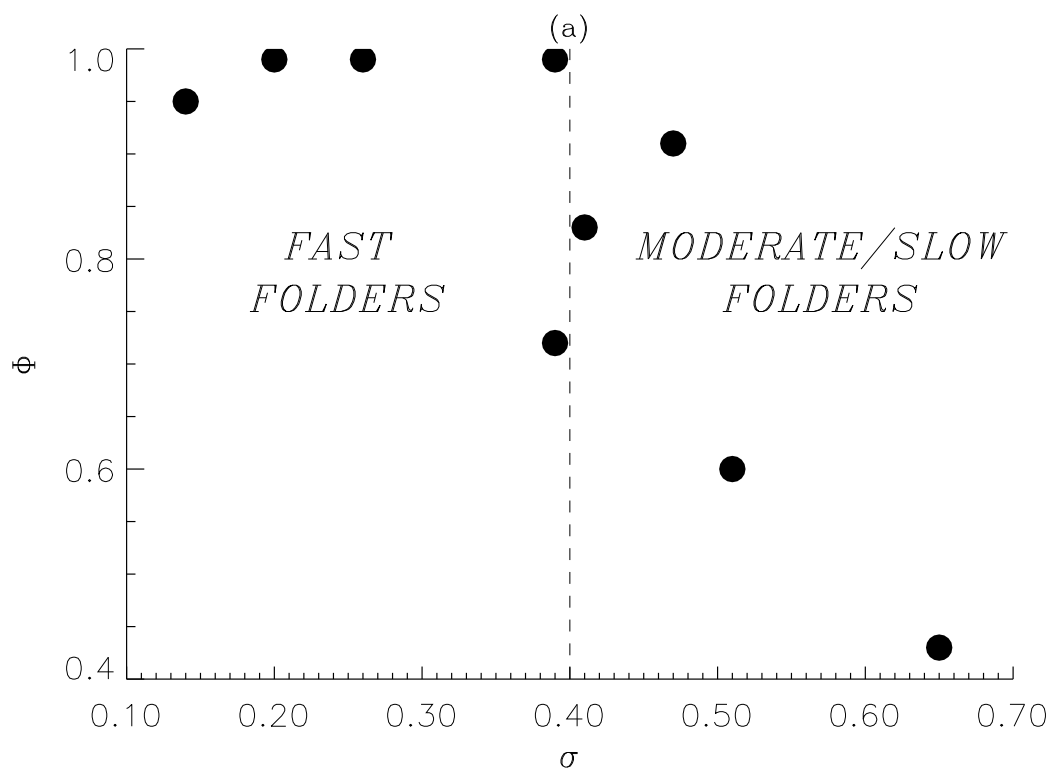
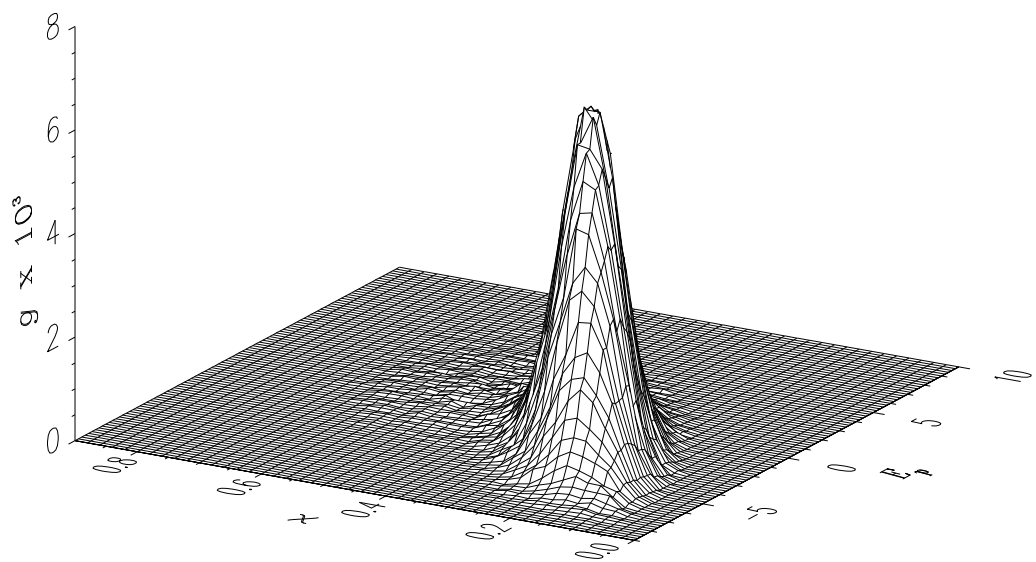


Fig. 9

(a)



(b)

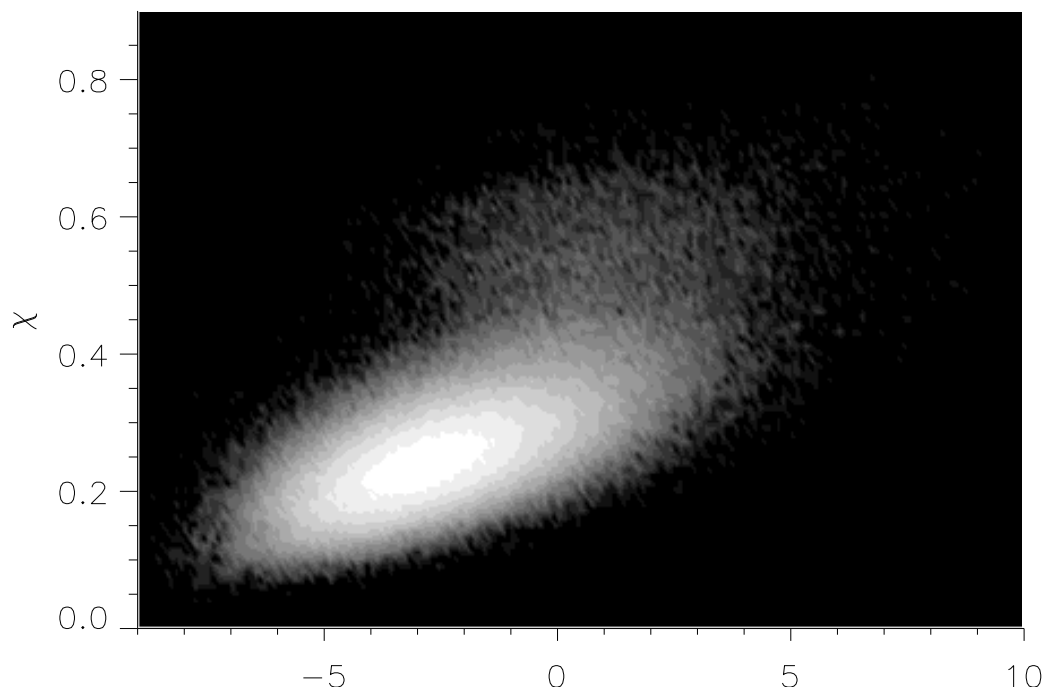
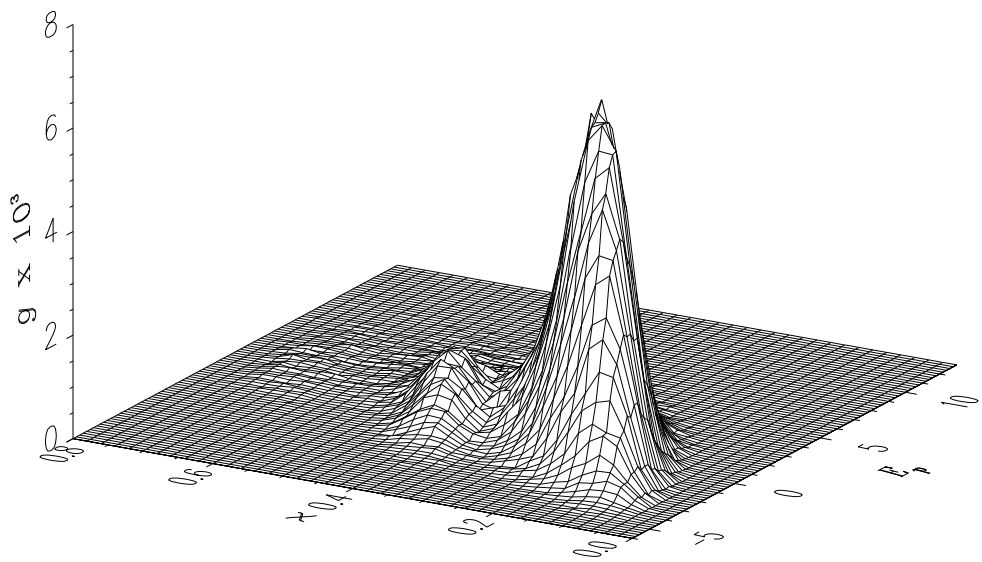


Fig. 10

(a)



(b)

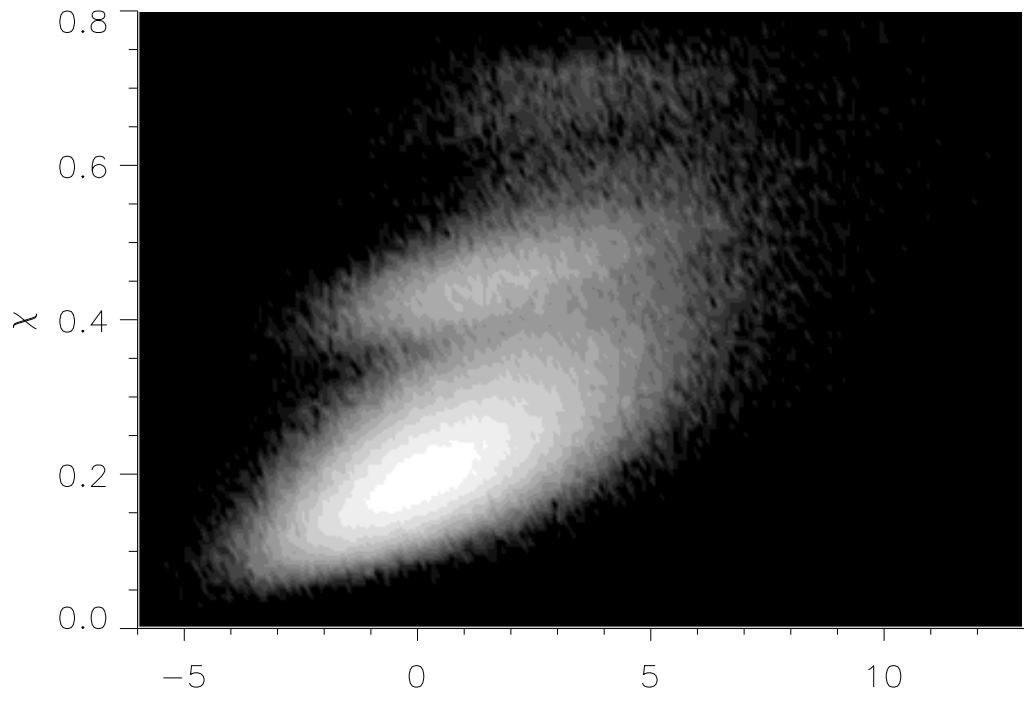
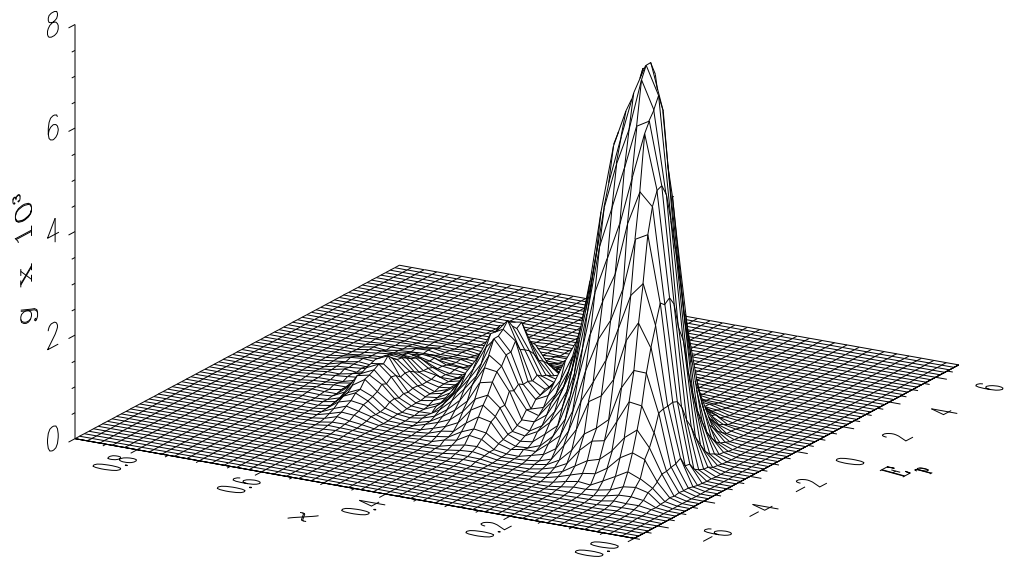


Fig. 11

(a)



(b)

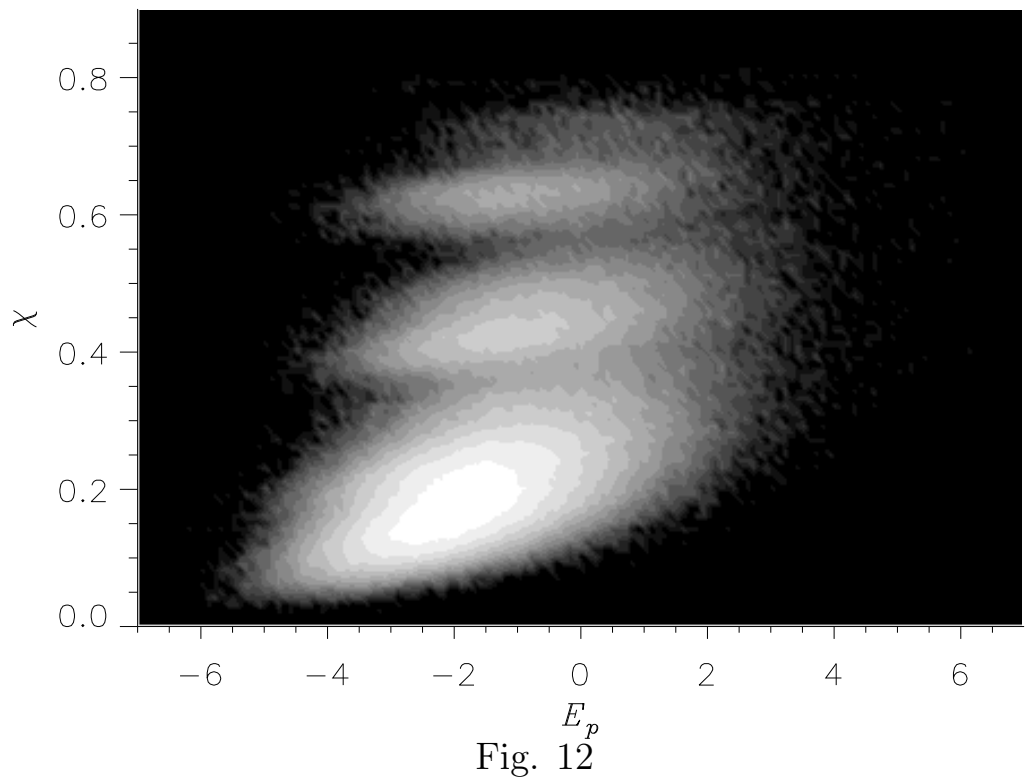


Fig. 12

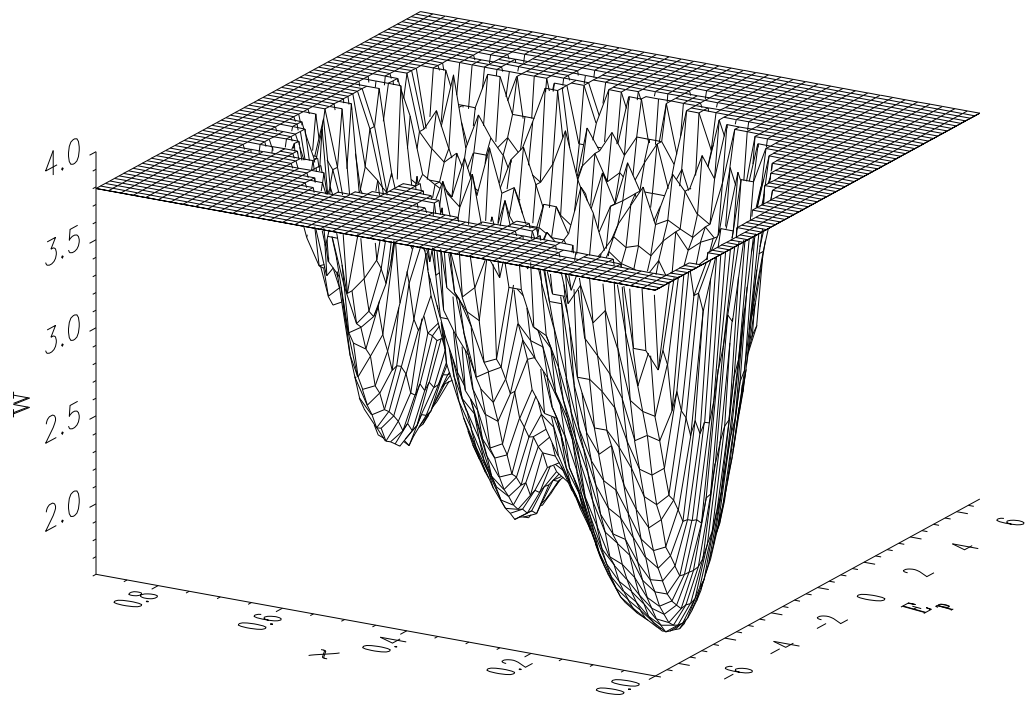


Fig. 13

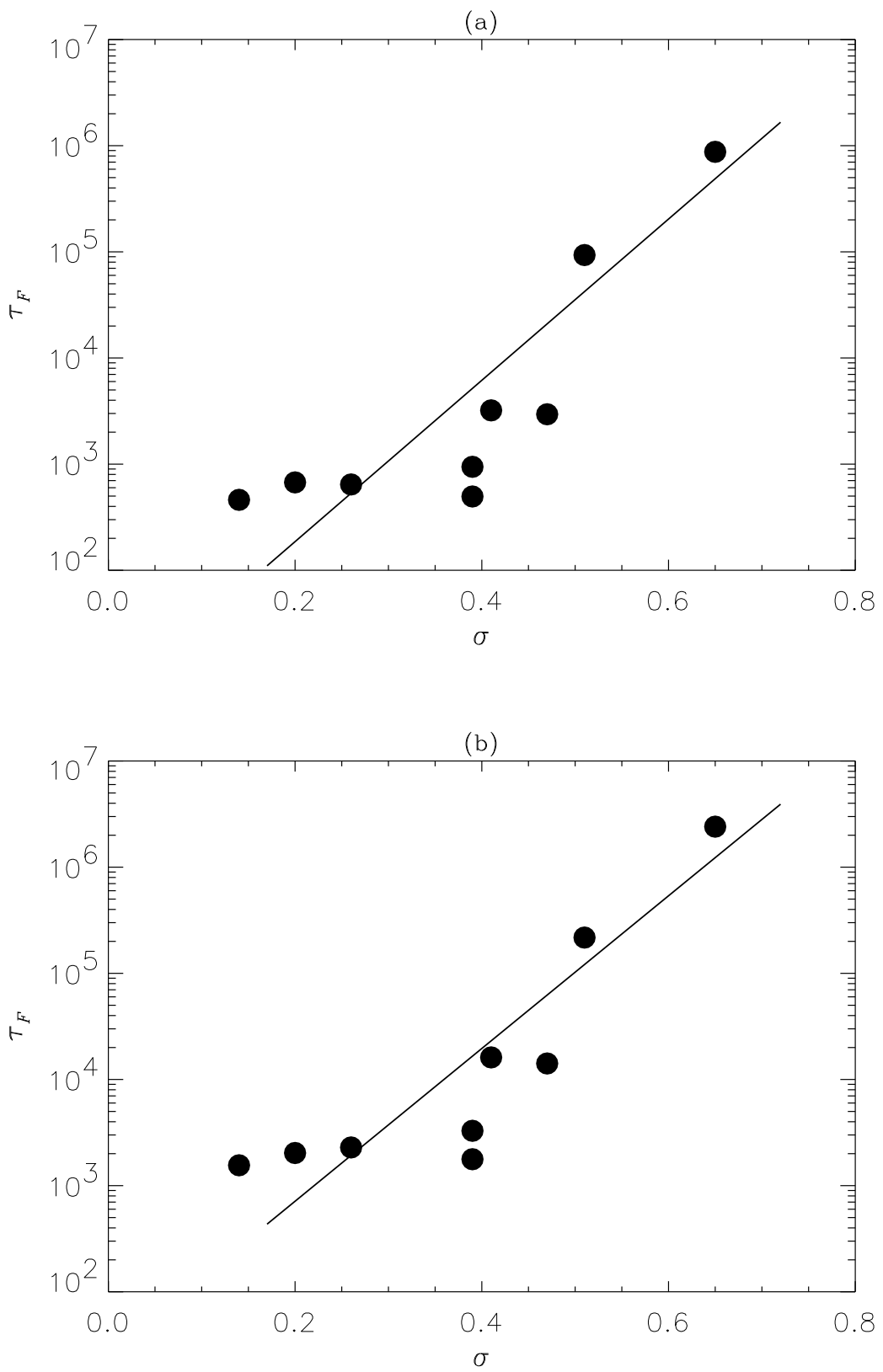


Fig. 14

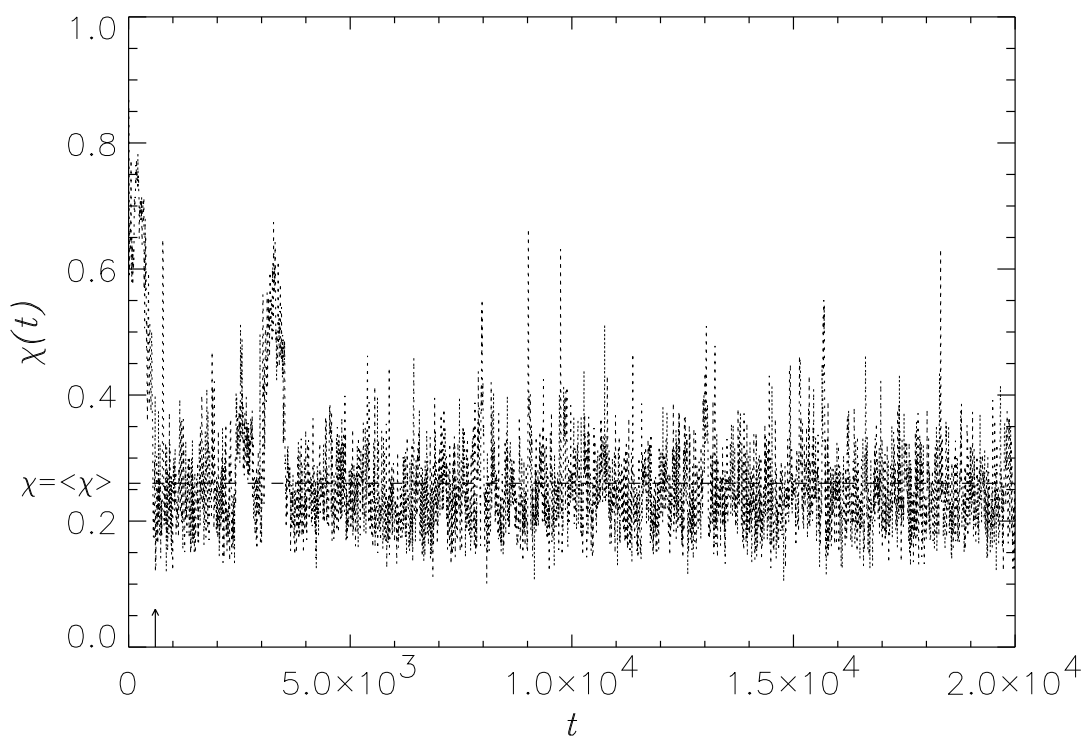


Fig. 15

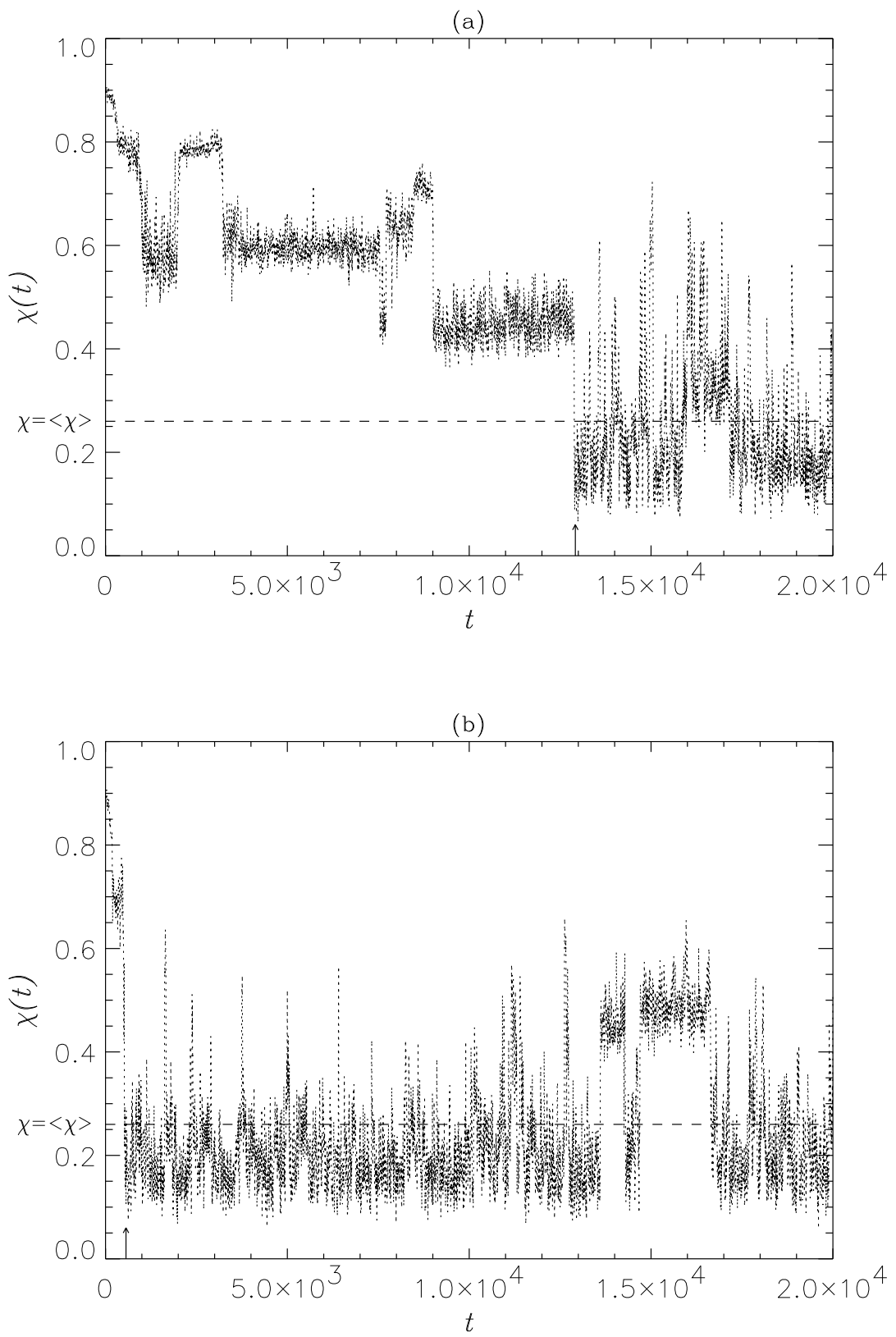


Fig. 16